separations

MDPI

Review

Recent Clay-Based Photocatalysts for Wastewater Treatment

Chitiphon Chuaicham [1], Jirawat Trakulmututa [1], Kaiqian Shu [1], Sulakshana Shenoy [1], Assadawoot Srikhaow [1], Li Zhang [1], Sathya Mohan [2], Karthikeyan Sekar [1,2] and Keiko Sasaki [1,*]

[1] Department of Earth Resources Engineering, Kyushu University, Fukuoka 819-0395, Japan
[2] Department of Chemistry, Faculty of Engineering and Technology, SRM Institute of Science and Technology, Kattankulathur 603203, India
* Correspondence: keikos@mine.kyushu-u.ac.jp

Abstract: Photocatalysis is a remarkable methodology that is popular and applied in different interdisciplinary research areas such as the degradation of hazardous organic contaminants in wastewater. In recent years, clay-based photocatalyst composites have attracted significant attention in the field of photocatalysis owing to their abundance, excellent light response ability, and stability. This review describes the combination of clay with focusing photocatalysts such as TiO_2, g-C_3N_4, and Bi-based compounds for degrading organic pollutants in wastewater. Clay-based composites have more active surface sites, resulting in inhibited photocatalyst particle agglomeration. Moreover, clay enhances the creation of active radicals for organic pollutant degradation by separating photogenerated electrons and holes. Thus, the functions of clay in clay-based photocatalysts are not only to act as a template to inhibit the agglomeration of the main photocatalysts but also to suppress charge recombination, which may lengthen the electron–hole pair's lifespan and boost degrading activity. Moreover, several types of clay-based photocatalysts, such as the clay type and main photocatalyst, were compared to understand the function of clay and the interaction of clay with the main photocatalyst. Thus, this study summarizes the recent clay-based photocatalysts for wastewater remediation and concludes that clay-based photocatalysts have considerable potential for low-cost, solar-powered environmental treatment.

Keywords: photocatalysis; TiO_2; g-C_3N_4; Bi-based-compounds; organic degradation

check for updates

Citation: Chuaicham, C.; Trakulmututa, J.; Shu, K.; Shenoy, S.; Srikhaow, A.; Zhang, L.; Mohan, S.; Sekar, K.; Sasaki, K. Recent Clay-Based Photocatalysts for Wastewater Treatment. *Separations* **2023**, *10*, 77. https://doi.org/10.3390/separations10020077

Academic Editor: Gavino Sanna

Received: 27 December 2022
Revised: 19 January 2023
Accepted: 20 January 2023
Published: 22 January 2023

Copyright: © 2023 by the authors. Licensee MDPI, Basel, Switzerland. This article is an open access article distributed under the terms and conditions of the Creative Commons Attribution (CC BY) license (https://creativecommons.org/licenses/by/4.0/).

1. Introduction

1.1. Photocatalysis and Its Mechanism

A potential global crisis has been brought to light in recent decades due to pollution and energy scarcity. In order to ensure the long-term success of human civilization, it is essential that progress be made in alternatives to polluting and energy-intensive processes as the need to clean up the environment is pressing [1–6]. Since the 1960s, there has been a growing emphasis on photocatalysis as a method for degrading organic contaminants [7,8]. It has been shown to have tremendous promise for CO_2 reduction, photocatalytic H_2 production, and water pollution purification as a low-cost and environmentally benign technology [9–12]. The photocatalyst is the key component of this technique since it turns solar energy into chemical energy, which, in turn, eliminates the pollutants [13–15]. Figure 1 is the schematic diagram illustrating the mechanism of photocatalysis [16].

Photoexcitation of electrons (e^-) and holes (h^+) happens when the energy of the incoming light is greater than a critical value. Photon energies are comparable to or greater than the semiconductor's band gap. Some of the e^- and h^+ at the surface of photocatalysts will interact with electron acceptors or donors. The e^- and h^+ may recombine nonradiatively or radiatively to generate, but they can also become stuck in shallow or deep traps. When exposed to heat or light, photocatalysts lose part of their photocatalytic efficiency [17–19]. The photocatalyst with poor photocatalytic efficiency in highly diluted solution has a low specific surface area and restricted adsorption capacity. In addition,

most nanometer-scale photocatalysts are not suitable for extensive industrial applications because they are challenging to separate in suspension. Therefore, it is crucial to produce photocatalysts with strong adsorption capacities and advantageous sedimentation qualities. Numerous materials, including silica, activated carbon, zeolites, and clays, have been utilized as supports for various semiconductors in an effort to improve their adsorption capacity and decrease their inclination to aggregate [20–22]. These support materials serve as active sites with a high surface area and porosity. Additionally, by making the components recoverable from the reaction mixture, the support material improves reusability by preventing material agglomeration.

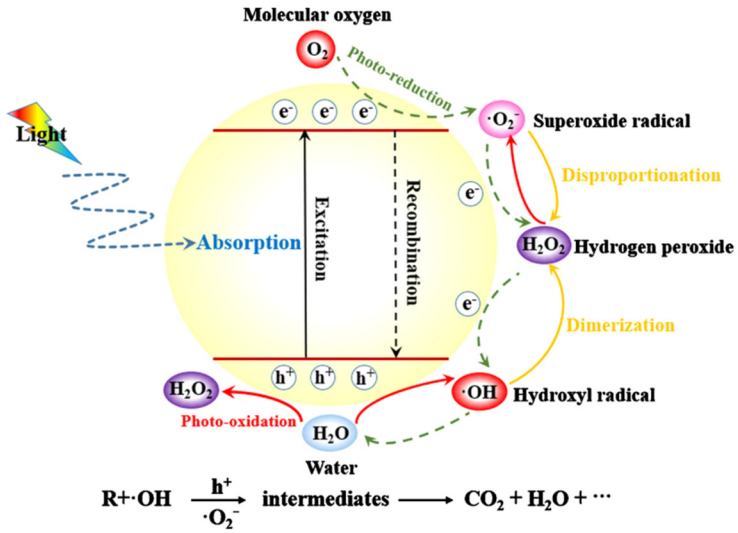


Figure 1. Schematic diagram illustrating the mechanism of photocatalysis. Reproduced with permission [16].

1.2. Type and Role of Clay in Photocatalysis

Clays are important in many areas due to their exceptional physiochemical features. These include excellent adsorption capacity, swelling property, biocompatibility, strong surface reactivity, and cation-exchange capacity. After their proven success as a semiconductor support for the catalytic degradation of various organic pollutants, layered (e.g., smectites) and fibrous (e.g., sepiolite) clays are seen as promising materials. Both cationic clays and anionic clays (such as stacked double hydroxides) could be used to describe the properties of clay materials. Clay minerals often include layers of aluminosilicate that are composed of one or two Si–O tetrahedral sheets and one Al–O (Mg–O) octahedral sheet. (Figure 2) [23]. Gibbsite and brucite are two examples of clay minerals, and they are categorized as either 1: 1-type or 2: 1-type depending on the number of stacked silica sheets (Figure 3) [24,25].

Since the early seventeenth century, kaolinite has been used as a material source for ceramic production in China. Kaolinite crystals can be found in a variety of phases, including triclinic, pseudomonoclinic, and polymorphs, as well as their ideal form, which is in the pseudohexagonal phase (dickite, nacrite) [26,27]. In a 1:1 ratio, gibbsite-like octahedral alumina and tetrahedral silica sheets are placed alternately. The chemical formula of kaolinite is $Al_2Si_2O_5(OH)_4$, while the hydrate form ($Al_2Si_2O_5(OH)_4 \bullet nH_2O$) can be defined as a halloysite structure. When wet, the strong binding forces between the layers in their structure prevent them from expanding [28,29].

Smectite and montmorillonite, weathered from soils, rocks (mostly bentonite), or volcanic ash, are categorized as 2:1 type clay minerals owing to their layer-by-layer octahedral sheet construction sandwiched between two tetrahedral sheets. Most of the layer charge originates from the cationic substitution of Mg^{2+}, Fe^{2+} for Al^{3+} in the octahedral sheet, or the replacement of Al^{3+} for Si^{4+} in the tetrahedral sheet. Interlayer cations that may be exchanged neutralize the ensuing negative layer charge. Mg^{2+}, Sr^{2+}, Na^{+}, K^{+}, and Ca^{2+} are all potential interlayer cations; nonetheless, Ca^{2+} and Na^{+} are the most prevalent. The

interlayer cations can be hydrated, and the creation of diffuse double layers by osmosis results in swelling behavior. Electrostatic force superimposes montmorillonite layers in an aqueous solution, and the gap between layers is typically 0.8–2.0 nm. Potential environmental contaminants may react in confined areas, increasing contact times between substances and, hence, reaction rates [26,27,30,31].

Vermiculite ($(Mg, Fe^{2+}, Fe^{3+})_3(SiAl)_4O_{10}(OH)_2 \bullet 4H_2O$), a hydrous phyllosilicate mineral, is also a member of the 2:1 group of expandable clay minerals that exfoliate significantly when heated. Due to the greater substitution of Al^{3+} in place of Si^{4+}, vermiculite has a higher layer charge density than the smectite group of clay minerals due to the strong negative charge on its tetrahedral sheet (between 0.6 and 0.8 per unit formula). Unlike smectites, the strong interlayer cation bonding binds the 2:1 layer together, limiting basal gap expansion to 1.5 nm. Vermiculite is especially well suited to bond with weakly hydrated cations such as K^+, NH_4^+, and Cs^+, due to its high charge per formula unit and strong cation-exchange capacity [26,27,30,31].

Mica and illite are two nonexpansive 2:1 clay minerals. They are a type of phyllosilicate, sometimes known as layered aluminosilicate. Muscovite, with the chemical formula $KAl_2(AlSi_3O_{10})(OH)_2$, is the most prevalent type of mica and can be found in a wide variety of rocks including granites, pegmatites, gneisses, and schists. Because of the presence of a central cation in their octahedral structure, the micas can be categorized as more structured, such as paragonite, biotite, and margarite. Illite clays are low in alkalies and contain a lesser proportion of Al substitution for Si when compared to the structure of muscovite. Therefore, the usual chemical formula for illite is $K_xAl_2(Al_xSi_{4-x}O_{10})(OH)_2$, where $x < 1$. Due to a charge imbalance, Ca and Mg can potentially be incorporated instead of K, leading to preventing H_2O from entering the structure [26,27,30,32].

Chlorite is a member of the 2:1:1 silicate group, which consists mostly of silicates of iron, magnesium, and aluminum. The typical chlorite clay crystal is formed of alternating layers of 2:1 and a magnesium-dominated tri-octahedral sheet (brucite-like sheet), resulting in a 2:1:1 ratio. Like the brucite layer, magnesium ions occupy all octahedral positions in chlorite. When compared to smectite or vermiculites, chlorites have a lower negative charge, but their negative charge is still similar to that of fine-grained mica. Due to the lack of water adsorption between the layers, this crystal does not expand. These structural features are conducive to substitution-based cationic exchanges, allowing for the electroneutrality of the layer to be maintained. Since the quantity and valence of the hydroxy-Al polymer living in the interlayer gap might vary, the cation-exchange capacity (CEC) of expandable 2:1 clay structures is reduced as a result. They incorporate mostly Mg, Al, and Fe cations in the octahedral sheets within the 2:1 layer and in the interlayer hydroxide sheets, with minor quantities of Cr, V, Mn, Li, Cu, and Ni cations. They also show a significant Si ion substitution for Al ion in the tetrahedral sheets [26,27,33].

In the hydrotalcite system, which includes the anionic clay known as layered double hydroxide (LDH), the brucite structure is very malleable owing to the compounds' adaptability in composition creation. LDH has a general formula of $[M^{2+}_{(1-x)}M^{3+}{}_x(OH)_2](A^{n-})_{x/n} \bullet zH_2O$, where $M^{(II)}$ and $M^{(III)}$ are divalent and trivalent metal cations to form positively charged metal hydroxide layers. Moreover, A^{n-} is an intercalated exchangeable anion and z is the moles of water molecules present in the interlayer space similar to anion [34,35].

In recent years, there has been a lot of research into the use of clay minerals as supports for various photocatalysts. The photocatalytic activity in photocatalysts is enhanced when the nanoparticles of photocatalysts are dispersed over the surfaces of clay minerals since this creates more active surface sites and reduces the agglomeration of photocatalyst particles. For example, halloysite, which is an aluminosilicate clay, was used as a template to coat selfpolymerized dopamine for the decomposition of the aforementioned pollutants [36]. Researchers have discovered that clays may boost the photocatalytic activity in nanoparticle photocatalysts. In addition, some impurities in clay such as Fe can enhance the optical properties of clay and tune a photoresponse activity in clay. For ex-

ample, when montmorillonite contained some Fe impurity, the function of this clay in a photocatalyst composite is not only to provide the site for the development of the main photocatalyst but it can also participate in the electron transfer mechanism to prevent the recombination of charge carriers [37]. Moreover, the surface contact between clay and the main photocatalyst is important for wastewater treatment. The large surface area of clay, such as two-dimensional or sheet structure clay such as montmorillonite, could provide more surface interaction between clay and the main photocatalyst than one-dimensional or pillar-like structure clay such as attapulgite and sepiolite, resulting in enhancing the separation of the electron and hole of the main photocatalyst.

Therefore, heterogeneous photocatalytic processes are receiving an increased amount of attention as a potential method for the degradation of organic contaminants mainly due to the fact that it is an effective method that is also cost-effective and kind to the environment for eliminating organic pollutants from the aquatic environment. [38–42]. Clay minerals have been used more often to prepare heterogeneous photocatalysts. Clay minerals such as montmorillonite, bentonite, kaolinite, hectorite, halloysite, and LDH have been utilized as supports. The impregnation of TiO_2 on the clay surface or between its layers is chosen for the manufacture of TiO_2/clay nanocomposites. Increased photocatalytic activity in TiO_2/clay nanocomposites is attributable to a decreased charge recombination rate [43–45]. Importantly, heterostructures that may operate as catalysts, such as semiconductor-type photocatalysts, can be developed by the functionalization of clay minerals in conjunction with inorganic nanoparticles [46]. Furthermore, here is a problem that should be taken seriously. Most industrial products are prepared in water. In fact, the energy and water needed to run such a process would be substantial. It would be more expensive and degrade the environment to deal with the wastewater. As a consequence, an effluent-free and energy-saving synthesis technology is absolutely necessary. In recent years, increasingly, much of the literature has already demonstrated that ball milling is a potential method to prepare photocatalysts [47–50]. In addition to being utilized for the photocatalytic breakdown of pollutants, clay-based photocatalysts can also be employed to produce H_2 or reduce CO_2. Additionally, these composite photocatalysts exhibit improved photocatalytic activities and are simple to recover from the solution as compared to pure semiconductor photocatalysts.

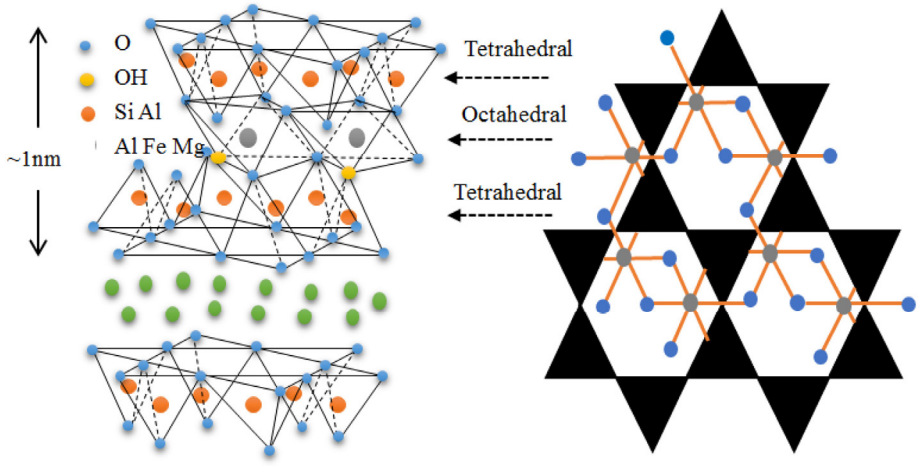


Figure 2. Different components of a basic clay structure. Reproduced with permission [51].

This paper is an effort to evaluate and consolidate current developments in the synthesis and photocatalytic uses of clay-based photocatalysts. Furthermore, the influence of the surface and structural properties of clay-based photocatalysts on their photocatalytic activity is explored. The prospects for the use of clay-based photocatalysts in environmental cleanup seem promising. In particular, this paper delves deeply into the function of clay materials in photocatalysis.

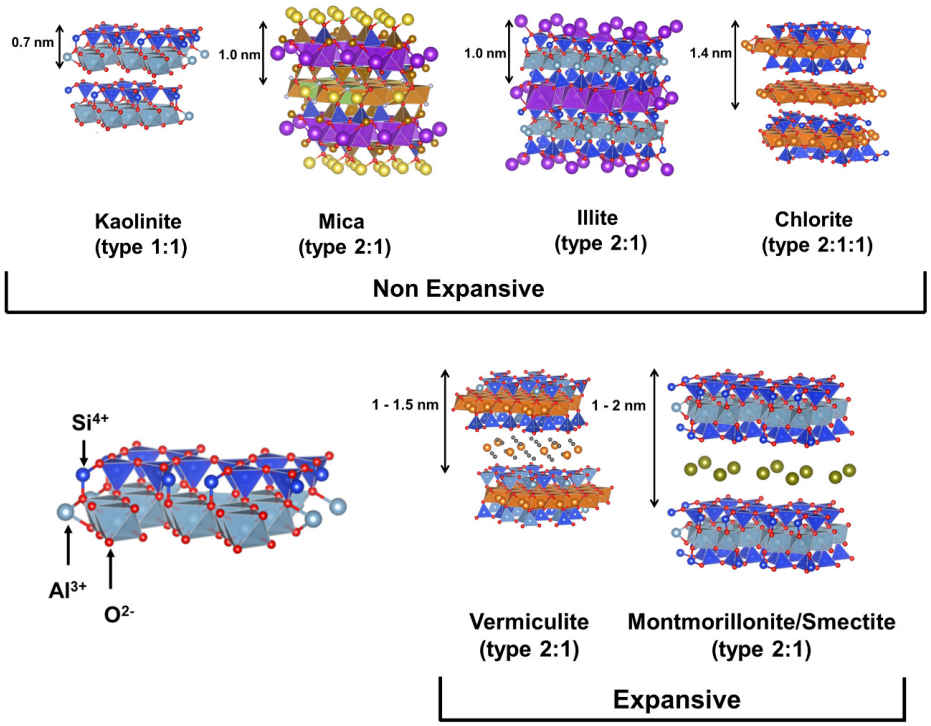


Figure 3. Atomic diagram of expansive and nonexpansive clays generated in VESTA program, using structural parameters from the Crystallography Open Database (COD) and arrangement of tetrahedral and octahedral layers in different clay types.

2. Clay-Based Photocatalyst

2.1. Graphitic Carbon Nitride/Clay Composites

Graphitic carbon nitride (g-C_3N_4) has attracted a lot of research interest as a metal-free photocatalyst due to its favorable band gap (2.7 eV), environmental friendliness, high stability, and ease of synthesis [52,53]. However, pure g-C_3N_4 has low photocatalytic activity because of its poor electron mobility, modest surface area, and rapid recombination of charge carriers [54,55]. Numerous solutions have been proposed to overcome the shortcomings of g-C_3N_4, such as heteroatom doping [56,57], decoration of noble metals [58,59], fabrication of heterostructures [60,61], and design of porous microstructures [62,63]. Although the methods described here are remarkably efficient, it is still crucial to developing simple and inexpensive synthetic methods to improve the photocatalytic performance of g-C_3N_4 in order to preserve the benefit of scale-up synthesis.

Natural clay minerals are abundant, inexpensive, and environmentally sustainable; some examples include talc, kaolinite, montmorillonite, and sepiolite [24,64]. Because of their one-of-a-kind topological chemical properties, they possess a large surface area and excellent adsorption; these qualities allow them to better disperse and perform as a photocatalyst [65]. It has also been reported that they can aid in photon absorption and their strong adsorption ability prevents charge recombination via the capture of charge carriers, thereby enhancing photocatalysis [66]. The 2D structures of clay minerals make it easier for them to bond with g-C_3N_4 and it has been reported that the photocatalytic efficiency of g-C_3N_4 can be greatly enhanced through the fabrication of g-C_3N_4/clay composites [67].

2.1.1. g-C_3N_4/Kaolinite

For instance, g-C_3N_4 shares the same layered structure as kaolinite and can be put together to create a sandwich structure. The kaolinite layer obtained by Sun et al. by a mechanochemical method had a combination of closely packed and regularly decorated 2D g-C_3N_4 nanosheets, resulting in a significantly rough surface. Natural kaolinite's layered structure not only provides a large surface area for the adsorption of pollutants but also

allows it to come into close contact with the g-C_3N_4 nanosheets in the composite. Under visible light irradiation, they found that kaolinite-supported g-C_3N_4 removes rhodamine B (RhB) at a rate that is four times higher than that of g-C_3N_4 alone. The synergistic effect between kaolinite and g-C_3N_4 created more adsorption and photocatalytic reaction sites, reducing the chance of recombining photoinduced electron–hole pairs [67].

Adding polar organics to the kaolinite intermediate layer creates an asymmetric space and a 2D microenvironment for insertion. The performance of charge transfer in photocatalysis can also be improved by using acid-modified polymers. Cyanuric acid was used as a modifier to make a modified-g-C_3N_4/kaolinite composite. After cyanuric acid modification, the surface of g-C_3N_4/kaolinite grew increasingly porous and homogeneous, which is likely what caused the thorough volatilization of cyanuric acid in the precursor throughout calcination. As the pores in its structure significantly enhanced, it resulted in an increase in the number of active sites for the degradation of pollutants [68].

Ternary composites with kaolinite have been extensively studied in photocatalysis, despite their more complex structure compared to that of binary composites. The unique 3D sandwich structure created by Li et al. (Figure 4a), which involved incorporating 2D g-C_3N_4 into a previously synthesized TiO_2/kaolinite structure, demonstrated a dramatically enhanced photocatalytic performance on organic pollutants degradation and bacterial inactivation (Figure 4b). Kaolinite in the composite improved the dispersion of TiO_2 and increased the exposure of g-C_3N_4 sheets due to its chemically bonded interfacial contact. The increased surface area and the increased ability to absorb visible light both contributed to the efficient generation of superoxide radicals [69].

In comparison to pure g-C_3N_4, the surface area and pore volume of the Fe/g-C_3N_4/Kaolinite photocatalytic composite prepared via the calcination method were both significantly larger, leading to a greater number of active sites and improved adsorption performance. With the photogenerated electrons being transferred to Fe^{III}, the Fe/g-C_3N_4/Kaolinite photo-Fenton system showed a superior degradation performance compared to photocatalysis and the Fenton reaction. Therefore, the efficiency of the Fenton reaction was increased while the consumption of H_2O_2 was decreased, resulting in a more stable and productive process [70].

Wang et al. synthesized g-C_3N_4/metakaolin composites that emitted 1.5 times more hydrogen than pure g-C_3N_4. The surface area was increased and the number of surface-active sites was multiplied due to the close contact between the two materials. Furthermore, the adsorption performance was enhanced, and the capacity to absorb visible light was increased which thereby resulted in increased photocatalytic performance [71].

2.1.2. g-C_3N_4/Attapulgite

Given its rod-like morphology, attapulgite (ATP), a type of natural silicate clay, has been widely used to create functionalized composites. In addition, it has a high number of hydrophilic groups and active sites, making it useful for the adsorption of a wide variety of pollutants. For instance, ATP was incorporated into the g-C_3N_4 structure by Zhu et al., and then the structure was embellished with quantum dots (QDs) of Fe_3O_4. The as-prepared Fe_3O_4@g-C_3N_4/ATP photocatalyst was the most successful in degrading 2-mercaptobenzothiazole. It achieved a percentage removal of 90.6% within only 90 min, which is twice as high as the removal efficiency achieved by pristine g-C_3N_4 (46%). The intercalation effect of ATP in g-C_3N_4 and the quantum effect of Fe_3O_4 QDs enhanced the light absorption ability and improved the separation efficiency of photogenerated electron–hole pairs which induced better conductivity between ATP and g-C_3N_4 [72].

In order to speed up the adsorption of $Cd^{(II)}$ in wastewater pollutions, Xie and coauthors reported a g-C_3N_4-modified attapulgite adsorbent via a simplistic freeze-drying-calcination method. Compared to commercially available adsorbents, the adsorption capacity of the synthesized g-C_3N_4/ATP adsorbents toward $Cd^{(II)}$ ions was shown to be significantly improved. The $Cd^{(II)}$ adsorption results were obviously consistent with the Langmuir model, which represents the monolayer adsorption process [73].

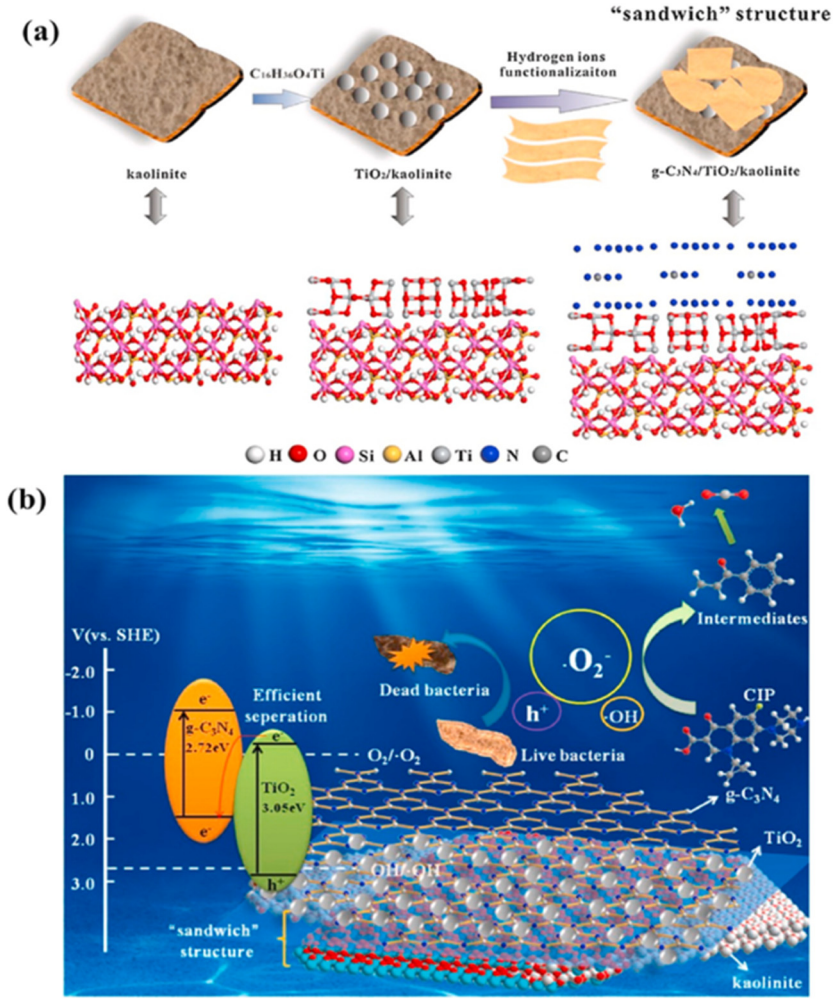


Figure 4. (**a**) Illustration of the synthesis process of g-C_3N_4 /TiO_2/Kaolinite composite. (**b**) Schematic representation of degradation mechanism using g-C_3N_4/TiO_2/Kaolinite composite under visible light. Reproduced with permission [69].

To create the Ag-assisted attapulgite/g-C_3N_4 composite, Xu et al. deposited Ag nanoparticles on the surfactant KH560 pregrafted g-C_3N_4-ATP. KH560 and melamine underwent a bimolecular nucleophilic substitution reaction, which resulted in the loading of a uniform g-C_3N_4 thin layer onto the ATP surface and the formation of a new chemical bond (Si–O–C). The pregrafted technique then kept the active Ag sites intact, allowing for the highly efficient localized plasmon resonance of the Ag nanoparticles. To prevent photogenerated electron–hole pairs from recombining during the photocatalytic degradation of methyl orange and to encourage the combination of oxygen and electron to form superoxide radicals, the accumulated electrons on the Ag nanoparticles further induced the formation of a Schottky barrier. This occurred rapidly due to the Ohmic contact between the ATP/g-C_3N_4 CB and the Ag nanoparticles as shown in Figure 5 [74].

2.1.3. g-C_3N_4/Halloysite Nanotubes

Halloysite nanotubes (HNTs) are nanotube-shaped clay minerals. Improvement in the stability of g-C_3N_4 is achieved through the immobilization of the photocatalyst on the halloysite support. Li et al. combined g-C_3N_4 with HNTs and ZnO through a novel calcination approach. The results of visible light photocatalytic experiments on a model antibiotic such as tetracycline show that the g-C_3N_4-ZnO/HNTs nanocomposites have significantly higher photocatalytic activity than either individual component. Because of a synergistic impact between the tubular support and the metals, nanocomposites that are

based on metals and supported on halloysite display a distinct electron transfer mechanism. This is made possible by the combination of the two components. In addition to its large specific surface areas and considerable adsorption capabilities, the hollow nanotubular shape makes it easier for reactants to diffuse into the photocatalyst, which in turn improves the photocatalyst's ability to absorb light via the process of light scattering. Additionally, its surface chemical structures, which include rolling silica tetrahedral layers and alumina octahedral layers with a higher conduction band edge, may modulate interfacial electron transfer dynamics. This results in an increase in the physical separation of injected electrons and a decrease in charge recombination reactions. Other properties of this material include a higher conduction band edge and rolling silica tetrahedral layers. Therefore, boosting charge migration at the nanointerface is responsible for better photocatalytic performance [75].

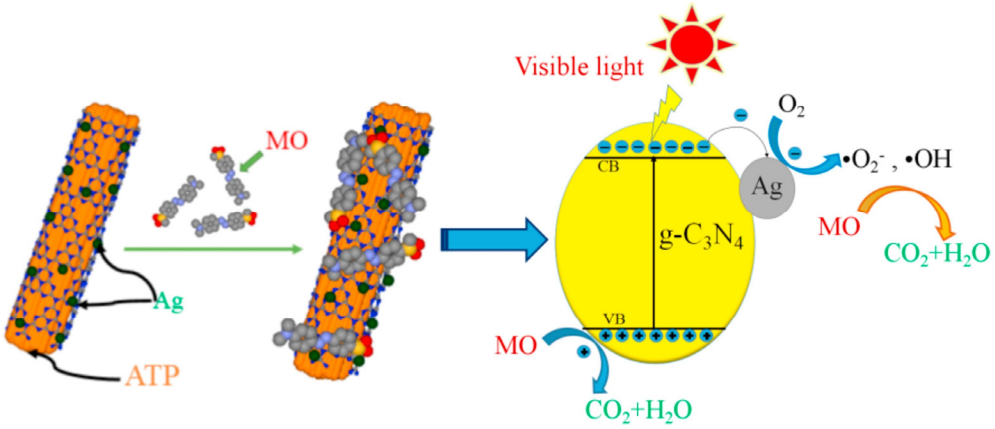


Figure 5. Schematic of the charge transfer mechanism of ATP/g-C_3N_4-Ag composite under visible light irradiation. Reproduced with permission [74].

By combining readily available g-C_3N_4 with $Ni(OH)_2$ nanoplatelets and earth-abundant halloysite nanotubes, a novel $Ni(OH)_2$@g-C_3N_4/halloysite nanocomposite was developed for use as a photocatalyst (Figure 6). When compared to g-C_3N_4 (0.43 μmolh^{-1}) and $Ni(OH)_2$@g-C_3N_4 (9.12 μmolh^{-1}), this ternary composite had the highest photocatalytic hydrogen evolution rate (18.42 μmolh^{-1}). Because of the negatively charged surface of HNTs, they are ideally suited for capturing photogenerated holes, and the positively charged surfaces of $Ni(OH)_2$ nanoplatelets allow for the efficient transfer of photogenerated electrons from the g-C_3N_4 to $Ni(OH)_2$ interface of the cocatalyst. Calculations based on molecular dynamics show that the adsorption of water and methanol molecules on the surface of this nanocomposite has the potential to be significantly improved. As a result, the nanocomposite's photocatalytic efficiency may be increased via the process of proton jumping [76].

2.1.4. g-C_3N_4/Montmorillonite

Montmorillonite has two tetrahedrally coordinated silicon sheets and one octahedrally coordinated aluminum sheet. It is anticipated that the assembly of g-C_3N_4 and montmorillonite into a 2D structure will eliminate the conventional drawbacks of pure photocatalysts. For example, it was reported by Li et al. that a strong interfacial contact could be achieved within a synthesized g-C_3N_4/montmorillonite composite through a simple two-step process, involving impregnation and calcination. The increased photocatalytic activity proved further that the composite could be used as a photocatalytic material for the removal of antibiotics and dyes from wastewater [77].

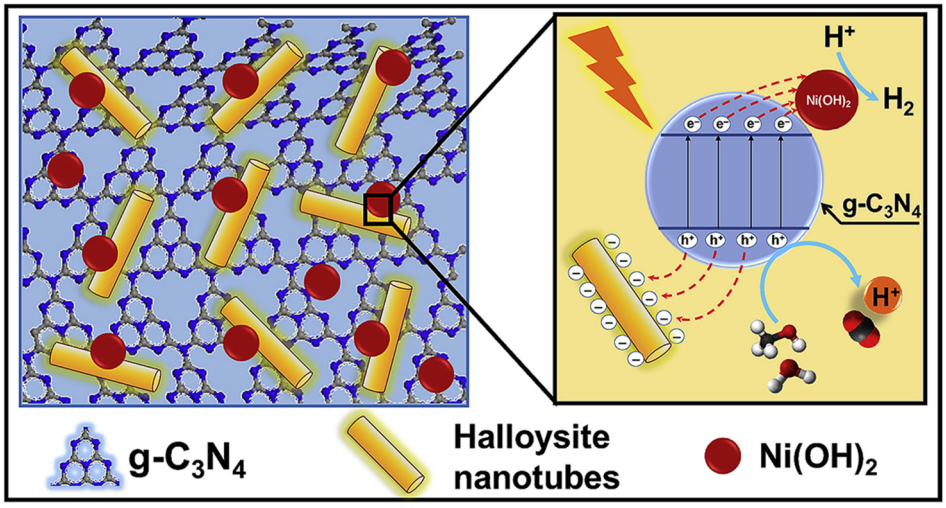


Figure 6. Schematic representation of separation and transfer of photogenerated charge carriers involved in the photocatalytic hydrogen evolution over the developed nanocomposite. Reproduced with permission [76].

The activation energy for the H_2 evolution reaction can be effectively reduced by g-C_3N_4 with suitable cocatalysts. Xu et al. used NiCoP as a cocatalyst to modify g-C_3N_4 hybridized montmorillonite, resulting in a cheap photocatalyst. The efficient spatial separation of electrons within the ternary composites, electrostatic repulsion from the negatively charged montmorillonite, and the light-harvesting ability of NiCoP all contribute to the remarkable H_2 evolution performance [78].

The adsorption efficiency for the removal of PO_4^{3-} and $Pb^{(II)}$ was studied by Wan and colleagues after they developed a novel composite of protonated g-C_3N_4 and acid-activated montmorillonite. After being assembled by the g-C_3N_4 layer, their surface structure became more disorganized and grainier. In addition, it had a specific surface area of 128.72 m^2/g. PO_4^{3-} and $Pb^{(II)}$ removal adsorption capacities were 5.06 mg/g and 182.7 mg/g, respectively [79].

2.1.5. g-C_3N_4/Rectorite

Rectorite, a naturally occurring mineral with a distinctive lamellar structure, may play a role in the formation of a 2D/2D morphological structure by inhibiting the agglomeration of g-C_3N_4 during the thermal polymerization process. A novel g-C_3N_4/rectorite composite was synthesized by Sun et al. using a simple and low-cost method. They found that including rectorite reduced g-C_3N_4 agglomeration, raised the surface area, and greatly enhanced the photocatalytic performance of the composite toward CIP degradation [80].

Recently, rectorite was developed to act as a carrier for g-C_3N_4 and improve the catalytic performance in the activation of peroxymonosulfate (PMS). At the same time, the rectorite had a confining effect, halting the aggregation of g-C_3N_4. The exposure of active sites is supposed to be enhanced, and the electron–hole recombination is stifled, by this. However, high concentrations of rectorite on the surface hydroxyl groups may play a direct role in the catalytic process, amplifying the reaction synergistically [81].

2.1.6. g-C_3N_4/Sepiolite

In order to facilitate the photocatalytic degradation of ciprofloxacin in the presence of visible light, a composite was developed consisting of natural sepiolite clay and synthetic g-C_3N_4 mixed with dispersed palladium nanoparticles. Their findings highlighted the potential contribution of the heterojunction between sepiolite and g-C_3N_4, as well as the Schottky barriers between g-C_3N_4 and Pd nanoparticles, toward the notable improvement in the photocatalytic performance of Pd nanoparticles/g-C_3N_4/sepiolite [82].

2.1.7. g-C_3N_4/Vermiculite

Vermiculite is an example of the 2:1 type of silicate mineral, which consists of sheets of silica oxygen tetrahedrons and sheets of aluminum oxygen or iron-oxide octahedrons that are coordinated with one another. Through a simple synthesis process, a novel g-C_3N_4/vermiculite composite with smaller g-C_3N_4 particles and enhanced photocatalytic properties was prepared. The microstructure and photocatalytic performance of the composite were studied to determine the optimum mass ratio of melamine to the expanded vermiculite. Vermiculite confinement of g-C_3N_4 particles, their close interfacial contact, and the electrostatic interactions between the two materials improved the photocarrier separation efficiency, photocurrent, and light absorption. These features, in addition to the reduced band gap, are what made the composite so effective as a photocatalyst [83].

By using acid-treated clay minerals and melamine as precursors, Chen et al. prepared clay mineral/g-C_3N_4 composites in a simplistic one-pot synthesis (Figure 7). The common clay minerals kaolinite, sepiolite, and talc were used as photocatalyst carriers. The CO evolution rate of the kaolinite/g-C_3N_4 composite was 3.03 $\mu molh^{-1}g^{-1}$ and the H_2 evolution rate was 385 $\mu molh^{-1}g^{-1}$, both of which were greater than the rates for g-C_3N_4 by a factor of 3.3 and 4, respectively. Light absorption, the number of active sites, and charge transfer were all improved in the composite because of its larger surface area and better distribution of g-C_3N_4 [84].

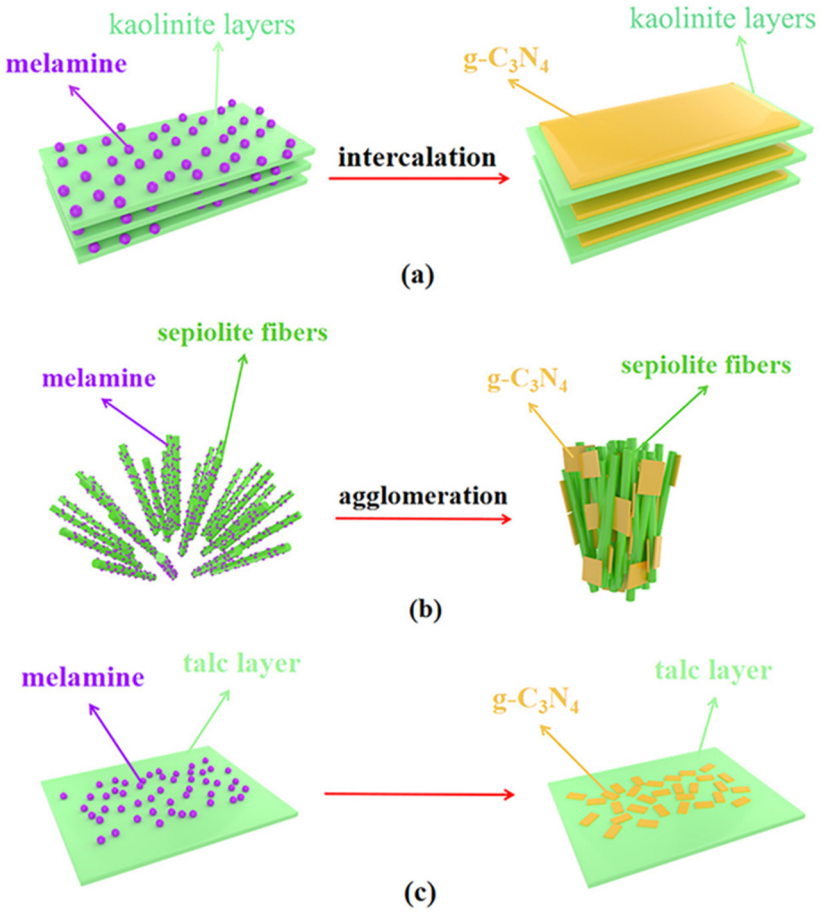


Figure 7. Synthesis of clay minerals/g-C_3N_4 composites (**a**) intercalation of g-C_3N_4 in kaolinite, (**b**) formation of g-C_3N_4 with sepiolite fibers and (**c**) formation of g-C_3N_4 with talc layer. Reproduced with permission [84].

2.2. Titanium Dioxide/Clay Composites

Titanium dioxide (TiO_2) has been reported as a photocatalytic electrode since the 1970s for water splitting under UV light irradiation [85]. Due to its light-harvesting properties,

TiO_2 adsorbs photon energy higher than its energy gap (E_g), which corresponds to each crystalline phase of TiO_2 (Anatase = 3.2 eV, Rutile = 3.0 eV, and Brookite = 3.3 eV) [85]. However, there are some limitations to using TiO_2 as a photocatalyst, such as UV-responsive semiconductor and the fast rate of photogenerated e^-–h^+ recombination [86]. Therefore, the composite fabrication between natural clay and TiO_2 is one of the effective methods to reduce the energy band gap and minimize the photogenerated e^-–h^+ recombination rate.

As a result of a high specific surface area, large pore volume, chemical stability, and commercial availability in large quantities, clay-based materials are promising to form the composite with TiO_2. The introduction of TiO_2 particles in the silicate layer of the clay minerals can change the adsorption behavior of these photocatalysts and different properties can be obtained for the photocatalytic reaction, depending on the surface properties of the host clay minerals. Since the 20th century, the composite between TiO_2 and natural clay (montmorillonite, kaolinite bentonite, and others) has been studied on photocatalytic remediation for several pollutants such as organic dyes, inorganic heavy metals, phenol, antibiotic waste, pesticides, and herbicides.

2.2.1. TiO_2/Montmorillonite or Smectite

In 2022, Yin Wang et al. reported the facile synthesis of zero-valent iron and copper at a nanoscale level that was intercalated over a montmorillonite nanocomposite which was extensively used for the reduction in $Cr^{(VI)}$, aiding in environmental depollution. In this system, copper was introduced as a catalyst to uplift the reactivity of Fe^0 which was then incorporated into montmorillonite (Figure 8). The combined effect of the as-synthesized material showed excellent catalytic activity toward the reductions in $Cr^{(VI)}$ and the relative effect of pH buffering of the clay material used had a significant influence over the removal efficiency and it varied through the run of the pH values. Studies of the above-said material revealed that a maximum removal of about 92.65% $Cr^{(VI)}$ was observed for pH 3 and it decreased significantly to about 59.43% at a pH 11 [87].

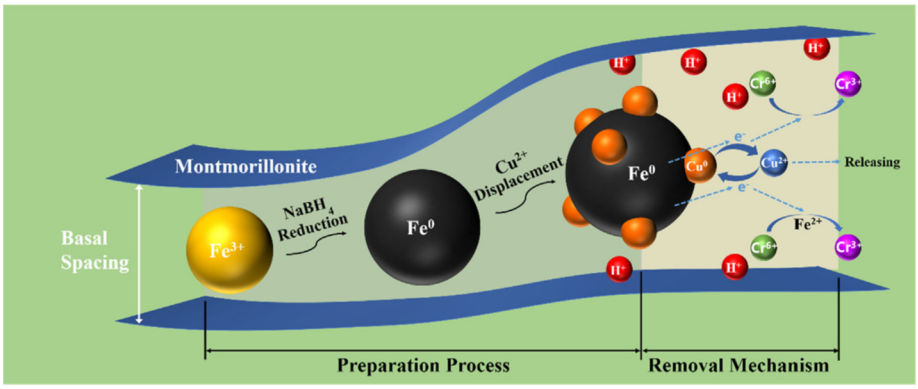


Figure 8. Removal mechanism of $Cr^{(VI)}$ using montmorillonite nanocomposite/TiO_2. Reproduced with permission [87].

Daimei Chen et al., in 2012, reported the facile synthesis methodology for the formulation of a montmorillonite clay composite that was supported with TiO_2. This anchored design of the material was designed using Ti alkoxides that were hydrolyzed with acid solutions in addition to polypropylene-supported di-quaternary salts (Figure 9). The morphological studies revealed that the TiO_2 particles were found to be well dispersed with nanoscale alignment with pillar-like fragments and the overall material was seen to be porous in nature and was found to be delaminated. The synthesized material was used for the degradation of methylene blue (MB) very efficiently. The composite exhibited 98% photocatalytic degradation efficacy toward MB within a time span of 90 min. This best removal was attributed to the improved porosity and surface area [88].

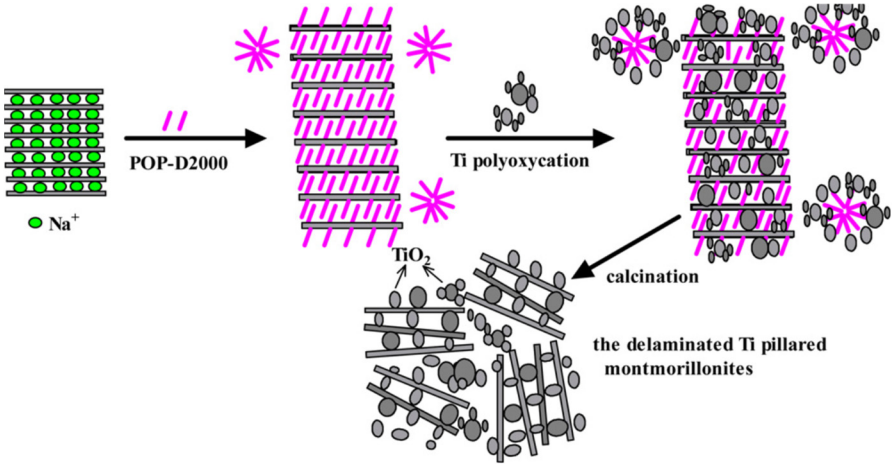


Figure 9. Delaminated structure of the montmorillonite pillared with Ti—Schematic representation. Reproduced with permission [88].

Li Zhang et al., in 2022, reported a temperature-varied photocatalyst with Fe-doped montmorillonite over TiO_2. The photocatalytic decomposition of phenol was studied with two variants, such as Fe/montmorillonite/TiO_2 wherein montmorillonite was doped with Fe^{III} and montmorillonite/Fe-TiO_2 where TiO_2 was doped with Fe^{III}, and the efficiency was found to be better for the former than the latter. In order to increase the activity in the photocatalyst, the fermi-level electrons were paired with the holes present in the valence band of the titanium dioxide, and so the recombination of electrons could be avoided to a maximum extent (Figure 10) [89].

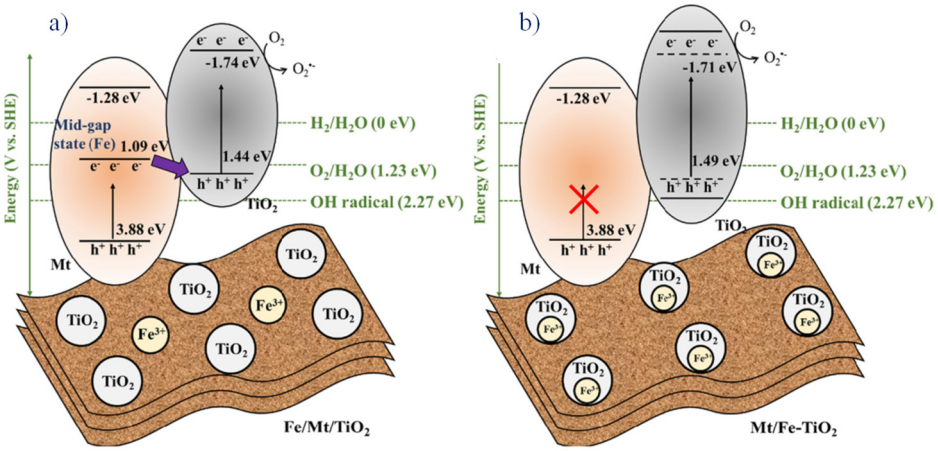


Figure 10. Charge transfer mechanism in two composites (**a**) Fe/montmorillonite/TiO_2 and (**b**) montmorillonite/Fe-TiO_2. Reproduced with permission [89].

V. Belessi et al., in 2007, studied the degradation efficiency and the characteristic behavior of TiO_2 dispersed over natural montmorillonite and synthetically prepared hectorite composite clay. This study was carried out to enhance the sorption capacity of TiO_2 toward the dimethachlor adsorption. Structural variations were found as the natural clay was seen to be aggregations of lamellar structures while that of synthetic clay was found to be delaminated with weak interactions. The surface characteristics such as pore volume and specific surface area were found to increase in the case of the increasing concentration of TiO_2 in the case of the montmorillonite while the contradiction was seen in the case of the hectorite. The reaction followed pseudo-first-order kinetics and the degradation efficiency was studied to be more dominant in the case of the composite/TiO_2 than that of the bare TiO_2 [90].

Julien G. Mahy et al., in 2022, reported the modification of natural smectite clay with TiO_2/ZnO to catalytically improve the efficiency of degradation. The as-prepared composite material was used for the degradation of p-nitrophenol and fluorescein. The photocatalytic efficiency was studied under UV light irradiation, and the material exhibited excellent activity of about 90% removal over a time of 8 h and the efficacy was profound in the case of p-nitrophenol [91].

2.2.2. TiO_2/Kaolin or Kaolinite

Mehdi Shirzad-Siboni et al., in 2022, reported the facile synthesis of zinc oxide which was being immobilized over kaolin clay material. This was achieved by the coprecipitation method wherein the synthesized ZnO was immobilized over the kaolin. This material showed excellent activity toward the reduction in $Cr^{(VI)}$ photocatalytically, and the removal percentage was reported as 88%. Interestingly, the influence of citric acid on the reaction system enhanced the catalytic activity and increased the removal percentage to about 98% [92].

Chunquan Li et al., in 2020, evaluated the formulation of TiO_2 dispersed over lamellar kaolinite through a rational design of the zero-dimensional and two-dimensional structural assembly. This novel material was used as an effective catalyst for the degradation of ciprofloxacin. Studies revealed that the enhanced catalytic activity in the as-synthesized catalyst was attributed to the cumulative effects of the natural clay composite along with the well-dispersed TiO_2 molecules. In addition to this, the synergistic effect led to a cocatalytic effect due to the proper dispersion of the TiO_2 particles and thereby enhancing the light-absorbing capacity of the catalyst as well. Moreover, all these effects added to regulations related to the lifetime of the carriers [93].

Xiaoyu Li et al., in 2018, reported the facile synthesis of a natural clay composite of kaolinite over TiO_2 and the work primarily focused on the dimensionality-based differences in accordance with their activity toward the tetracycline hydrochloride degradation. The flaky structure mentioned as FK/TiO_2 exhibited a supreme efficiency toward the degradation of the tetracycline hydrochloride and the reason stated was that the flaky structure had a higher adsorption capacity and the particle size was much smaller in addition to which the loading efficiency was also higher in comparison to the nanorod structure and the bare TiO_2. While looking at the structural properties, the two-dimensional nanoflakes structure had a stronger contact in the interfacial region attributed to the enhanced stability of the material [94].

K. Mamulova Kutlakova et al., in 2011, synthesized a photoactive composite of kaolinite/TiO_2 for the effective discoloration of acid orange in an aqueous solution. The work implemented the technique of calcination to produce meta kaolinite from kaolinite at 600 °C. The results concluded that the calcinated material was found to show a higher degradation efficiency in comparison to the dried one. The reason might be due to the prominent decrease in the amount of sulfur which was actually caused due to the absorption of free sulfuric acid over the surface of TiO_2. Latent hydraulic property and superior photocatalytic activity were the two beneficial factors of this material [95].

Yalei Zhang et al., in 2011, reported a simple synthesis method for the preparation of a mixed ternary composite based on TiO_2/kaolinite. The composite was known to show excellent photocatalytic activity toward the degradation of acid red G (ARG) and 4-nitrophenol (4-NP). A temperature of 70 °C was found to be the most prominent temperature for the highest photocatalytic efficiency toward the degradation of ARG and 4-NP. The highest efficiency was found in the binary mixture composite system containing anatase and brookite. The reported efficiency of the composite was attributed to the enhanced specific surface area and the heterojunction existing in the system [96].

Aichun Wu et al., in 2019, reported a facile sol-gel method to load nanoparticles of titanium dioxide over three different kinds of clay composites, namely, kaolinite, palygorskite, and halloysite, with different morphological variations prepared. The morphology was as plates, rods with micro tunnels, and tubes, respectively, and the prepared material was

studied for the degradation of methyl orange (MO) (Figure 11). The results were associated with the amounts of TiO_2 in different clays, wherein over the palygorskite surface, the agglomeration of TiO_2 nanoparticles was observed, and in halloysite, a much smaller amount of TiO_2 was seen on the tubes, attributing to the lower efficiency. Whereas kaolinite tended to provide a higher activity attributed to the higher adsorption of methyl orange to the hydroxyl surfaces, hence, kaolinite provided superior support to TiO_2 and the system was found to be stable [97].

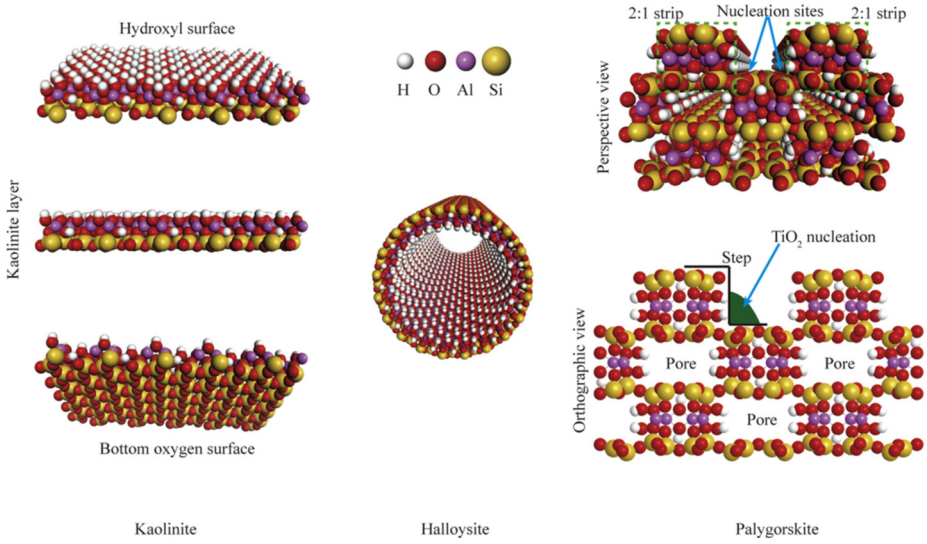


Figure 11. Diagrammatic representation of the mechanism of degradation of MO on the kaolinite surface. Reproduced with permission [97].

2.2.3. TiO_2/Bentonite

Ridha Djellabi et al., in 2016, studied the effect of TiO_2 with respect to its concentration over a bentonite clay composite and its consecutive action toward the removal of crystal violet and $Cr^{(VI)}$ when irradiated with sunlight. The study revealed the effects of the TiO_2 concentration having a major impact on the application and stated that an increase in the concentration of TiO_2 decreases the porosity of the material gradually. In respect to pollutant removal, the characterizations showed that both adsorption and photocatalytic activity clubbed together to remove crystal violet content from water, while in the case of $Cr^{(VI)}$, adsorption contributed on a lower scale and the removal was highly attributed to the photocatalytic effect which was, in turn, stated due to the increase in the concentration of TiO_2 in the material. The removal of $Cr_{(VI)}$ was associated with the adsorptive activity, attributing to the results of the zeta potential value which clearly depicted that the amount of negative charge was decreased due to the increase in the concentration of TiO_2 and, hence, the activity was due to adsorption rather than photocatalytic activity [98].

Chao Yang et al., in 2015, evaluated a method for the removal of methylene blue by preparing a TiO_2-WO_3-bentonite composite. This was performed by a simple hydrothermal method in addition to ultrasonic pretreatment. In comparison with the raw clay materials, the composite exhibited excellent surface area increases, and the ultrasonic pretreatment led to an increase in the exfoliation capacity and also the dispersion of TiO_2 increased, leading to higher activity toward the adsorption of MB. Further morphological studies and stability studies revealed that the increase in temperature had a greater impact on the adsorptive capacity as the raise in temperature decreased the adsorption ability [99].

Ithiara D. Dallabona et al., in 2021, used a floating alginate bead possessing TiO_2 and an organo-bentonite along with $CaCO_3$. This floating composite was used in the removal of tartrazine (TZ) and MB. The efficiency of removal was found to be 23.5% and 59.0% corresponding to TZ and MB, and it rose to a value of about 95% and 99% of TZ and MB when irradiated with UV light. The material was found to present good stability over seven

consecutive cycles, maintaining an efficiency of about 80%, which was attributed to the fact that TiO_2 was found to be available at the interface layer of water and air [100].

2.2.4. TiO_2/Zeolite

Qing Sun et al., in 2015, fabricated a simply hydrolysis-based synthesis of TiO_2 supported with natural zeolite. The hydrolysis process was followed by a series of temperature-varied calcination processes and the studies revealed the effect of the calcination temperature on the adsorption and photocatalytic efficiency of the material to degrade $Cr^{(VI)}$. Due to the highest specific surface, the adsorption was found to be optimum at 300 °C of the calcination temperature and the system followed pseudo-second-order kinetics. When the temperature was raised to 500 °C, the zeolite was able to retain its original structure and the adsorption capacity was also enhanced. Moreover, the removal efficacy of the sample was also seen to be stable at more than 75% after five consecutive cycles and, hence, the catalyst was said to be stable and durable enough for the degradation of $Cr^{(VI)}$ [101].

2.2.5. TiO_2/Serpentine

Zhiming Sun et al., in 2013, opted for a hydrolysis-deposition method for the facile synthesis of TiO_2 supported over acid-leached serpentine tailings. The synthesized catalyst was capable of reducing $Cr^{(VI)}$ which was due to the high specific surface area and the porous structure of the sample. In addition, there were huge hydroxyl groups present on the surface of the composite which resulted in higher adsorption of the target molecule $Cr^{(VI)}$. The prepared composite was capable of photocatalytically decomposing $Cr^{(VI)}$ with a removal rate of about 95% within a time span of 2 h and the material was found to be stable and reusable [102].

2.2.6. TiO_2/Layered Double Hydroxides

Yanting Yang et al., in 2019, employed a simple sol-gel method of the fabrication of a composite composed of TiO_2 and Zn-Al-layered double hydroxides (LDH-TiO_2). With the as-synthesized material, both the adsorption and photocatalytic efficiency were studied, wherein the results revealed that, for an amount of 20 mg/L of the model pollutant $Cr^{(VI)}$, the adsorption capacity ranged from about 26% to 75%, respectively. While that of the photocatalytic removal upon irradiation with UV light went up to a drastic removal percentage of about 100%. This varied activity in the material was in accordance with the amount of TiO_2 being incorporated. With the increase in TiO_2, the photocatalytic ability was increased and that of the adsorption was decreased. The kinetic studies evaluated for the reduction in $Cr^{(VI)}$ explained that the reaction followed a pseudo-second-order reaction [103].

2.2.7. TiO_2/Sepiolite

Fen fang Li et al., in 2015, reported the facile synthesis of a novel photocatalyst wherein sepiolite, a clay composite, was modified magnetically and was supported over TiO_2. The synthesis methodology followed the sol-gel method and studies revealed that the TiO_2 was found to appear in its anatase phase and the composite exhibited an excellent photocatalytic and adsorption capacity, and that it degraded 90.9% of 2,4-dichlorophenol (DCP) within 120 min under UV irradiation. In addition, in the binary state, the photocatalytic treatment showed up the enhanced removal of $Cr^{(VI)}$ and DCP at a removal efficiency of 100% and 96.9%, respectively. As a result, the removal of the pollutant was found to be effective due to the magnetic effect of the sepiolite supported with TiO_2 which was attributed to the synergistic effect persisting among the redox reactions taking place in the photocatalyst [104].

2.2.8. TiO_2/Romanian

E. Dvininov et al., in 2009, synthesized various compositions of Romanian clay pillared with TiO_2. The as-prepared material was capable of degrading congo red (CR) dye

efficiently under UV light irradiation. The increase in the photocatalytic efficiency of the material was in accordance with the size of the pillars of TiO_2 which, in turn, helped in uplifting the contact area in the interlayers, that is, between the dye solution and the photoactive species. The interlayers were expanded primarily by using cetyltrimethylammonium bromide (CTAB) wherein the intercalation between the negatively charged layers and cations was performed by modifying the clay composite into sodium form [105].

2.2.9. TiO_2/Diatomite

Zhiming Sun et al., in 2014, involved a hydrolysis-deposition method carried out under low temperatures for the preparation of a TiO_2/purified diatomite composite material for the photocatalytic degradation of RhB. The as-synthesized material showed a good photocatalytic removal of RhB under UV light irradiation wherein the efficacy was mainly attributed to the uniform dispersion of the nanoparticles of TiO_2 on the diatomite surface and the optimum grain size of the nanoparticles [106].

2.2.10. TiO_2/Anthracite

H. S. Ramadan et al., in 2021, reported a facile synthesis method for the impregnation of TiO_2 into anthracite that was modified with H_2O_2. This material was employed for the degradation of malachite green which worked best at 22–55 °C. The percentage removal efficacy was calculated for the removal of the modified anthracite at 49.8% and rutile at 71.4% while that of the composite was found to be 96.2%, respectively, and the efficiency was achieved at pH 8. The as-synthesized adsorbent was found to be stable for up to five cycles and the capacity of removal was calculated as more than 80% toward malachite green (MG) adsorption [107].

Moreover, the effect of pH in the TiO_2/clay composites was investigated for organic-containing wastewater. It can be found that the TiO_2/clay composites such as sepiolite-TiO_2 composite [108], TiO_2-montmorillonite composites [109], and TiO_2- bentonite composites [110] showed the highest photocatalytic activity for organic decomposition around neutral to basic pH conditions; however, the acid condition was not suitable for the photocatalytic organic decomposition due to the high stability of the clay composites. Normally, a low pH has a negative impact on the stability of clay particles because acid destroys the clay particles at their edges, causing the release of Al ions. Because of the influence that pore fluids have on pH, the thickness of the diffused double layer will be reduced; as a result, the clay particles will become thicker, which will result in a lower liquid limit [111].

2.3. Bismuth-Based Photocatalysts/Clay Composites

Recently, there has been a lot of interest in bismuth-based photocatalysts because their charge carrier density is low and the mean free path of the carriers is long. In addition, they offer a sizable contact space for other typical catalysts. In the treatment of organic wastewater, visible light-driven photocatalysts such as 2D-bismuth oxyhalides (BiOX, X = Cl, Br, I) are used due to their strong photoresponse in the visible light region, excellent photocatalytic activity, and simple synthesis. Bismuth vanadate ($BiVO_4$) has received considerable attention from researchers as an economical, environmentally benign n-type bismuth semiconductor because of its modest band gap (E_g = 2.4–2.5 eV), high stability, and efficiency in the removal of organic pollutants under visible light. Moreover, in recent years, the Aurivillius family member bismuth molybdate (Bi_2MoO_6) has received a significant amount of attention due to its impressive array of inherent features. Moreover, new findings reveal that Bi_2MoO_6, with its lower band gap energy (2.6 eV), is effective as a visible light-driven photocatalytic material for the degradation of organic substances. However, pure bismuth-based photocatalysts are limited in their applications because of the significant photogenerated charge carrier recombination that reduces their activity. Several different improvements to charge carrier separation have been documented so far thanks to changes in bismuth-based photocatalysts, including structural design, element doping, and heterostructure constructions. Currently, bismuth-clay-based photocatalysts

have gained significant interest, including in the development of photocatalyst materials because the high stability specific and surface area of clay avoid the agglomeration of bismuth-based photocatalysts. Furthermore, the separation of photogenerated electron–hole pairs is also improved by the heterojunction of clay and bismuth-based photocatalysts, leading to increased photocatalytic activity.

2.3.1. Bismuth-Based Photocatalysts/Montmorillonite

One of the most common clay minerals is montmorillonite, and each of its three-layer structural units consists of two silica tetrahedral sheets and a center alumina octahedral sheet. The enhanced surface area and pore volume are the two main benefits of modified montmorillonite. Two-dimensional photocatalysts based on bismuth may be combined with montmorillonite to form composite materials with enhanced photocatalytic activity. By using simple heating and impregnation techniques, Tun et al. created Ag NPs loaded with Bi_2O_3/montmorillonite nanocomposites (Figure 12). The Ag-loaded Bi_2O_3/montmorillonite nanocomposite was shown to have a considerably increased visible light-driven photocatalytic activity for tetracycline (TC) antibiotic and RhB degradation compared to those of Bi_2O_3 and montmorillonite, separately [112]. The increased photocatalytic activity in the Ag-loaded Bi_2O_3/montmorillonite nanocomposite is likely due to these properties. Due to montmorillonite's facilitation of a high specific surface area and the formation of additional active sites, the nanocomposites are able to be recovered from the reaction solution with remarkable efficiency.

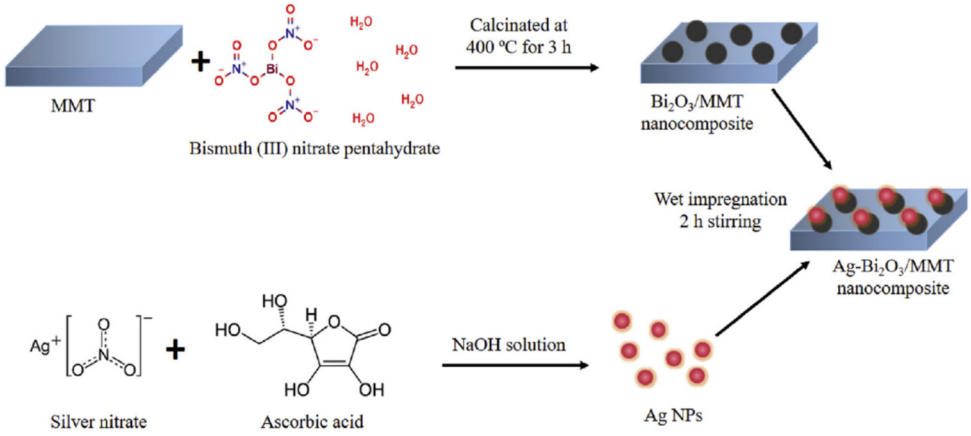


Figure 12. Schematic diagram of the synthesis process of Ag NPs loaded with Bi_2O_3/montmorillonite nanocomposites. Reproduced with permission [112].

In addition, CTAB was used as the Br source and template in the preparation of BiOBr/Na-montmorillonite composites (BiOBr-Mt) in a laboratory under ambient circumstances [113]. Na-montmorillonite with CTAB added can regulate BiOBr particle size, which is an intriguing discovery. In comparison to pure BiOBr, the BiOBr-Mt sample exhibited a higher photocatalytic activity for RhB degradation due to its substantial photoabsorption in the visible light band. The effective separation of photogenerated electron–hole pairs, synchronous role or coupling effect of adsorption and photocatalysis on the BiOBr-montmorillonite composites, and significant photoabsorption in the visible light area all contribute to the improvement in the photocatalytic activity.

Naing et al. used a one-step hydrothermal technique to produce BiOCl nanosheets doped with in situ reduced bismuth [114]. When exposed to visible light, the Bi/BiOCl/montmorillonite photocatalysts that were created showed increased photocatalytic activity for the degradation of RhB and TC. Adding montmorillonite as a supporter to the enhanced photocatalyst greatly increased its capacity to absorb pollutants. The semimetallic bismuth nanoparticles' surface plasmon resonance (SPR) effect on the BiOCl nanosheets widened the photocatalyst's light-absorbing spectrum. Visible light-driven synthetic photocatalysts

benefit greatly from the synergistic impact of semimetallic bismuth and montmorillonite, which promotes the separation of photogenerated electron–hole pairs.

In addition, montmorillonite was effectively combined with BiOCl to form BiOCl-montmorillonite. Effective photocatalytic degradation of RhB and orange G (OG) has been observed using BiOCl-montmorillonite exposed to UV light [115]. Surface Bronsted acidic sites and dissolved oxygen were found to enhance the expected processes responsible for the aforementioned efficient breakdown (Figure 13). As a result, montmorillonite had no effect on the aggregation of BiOCl particles, but the resulting BiOCl-montmorillonite composites were chemically stable. The heterogeneous photocatalytic degradation process was shown to be improved by combining BiOCl with Na-montmorillonite to generate BiOCl-montmorillonite.

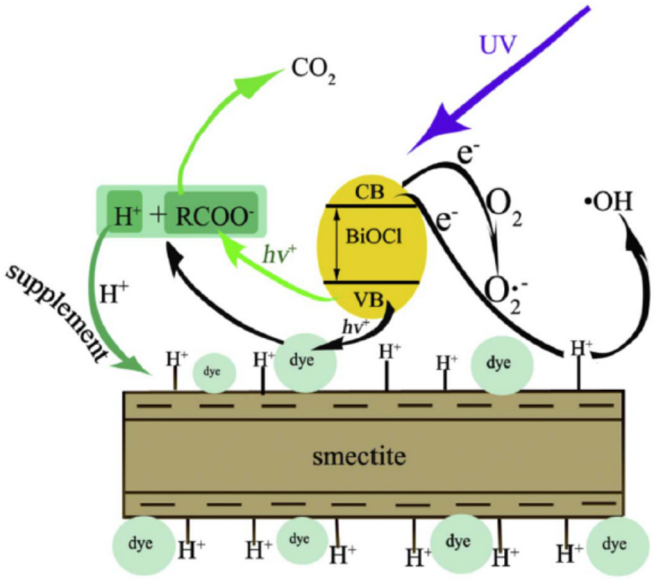


Figure 13. The potential photocatalytic reaction mechanisms or removal pathways responsible for the dye degradation over BiOCl-montmorillonite. Reproduced with permission [115].

In order to create a $BiVO_4$/Fe/montmorillonite composite with a high photo-Fenton catalytic activity for the degradation of acid red 18, Xu et al. established a technique for loading bismuth vanadate (BiVO4) on hydroxy-iron pillared montmorillonite (Fe/montmorillonite) [116]. Fe^{3+} on $BiVO_4$/Fe/montmorillonite was able to receive the photoinduced electrons from BiVO4 and be reduced to Fe^{2+}, producing the desired effect. With this decrease, electron–hole recombination is inhibited, and $BiVO_4$'s catalytic activity is boosted. The decomposition of H_2O_2 into highly oxidative •OH may also be sped up by irradiating it with visible light, which causes Fe^{3+} to be rapidly reduced to Fe^{2+}.

2.3.2. Bismuth-Based Photocatalysts/Bentonite

Due to its superior photocatalytic degradation activity for the organic pollutant in wastewater, bentonite composite has garnered attention alongside montmorillonite composites. For the photocatalytic degradation of CR, Landge et al. created a new S-scheme Bi_2O_3-ZnO based on bentonite clay nanocomposites by sonochemical synthesis [117]. The improved catalytic performance in Bi_2O_3-ZnO/bentonite clay may be attributed to the S-scheme mechanism of charge transfer between ZnO and Bi_2O_3, which occurs as a result of the increased redox potential of the latter. The addition of Bi and the support of bentonite clay to ZnO nanoparticles may also contribute to the excellent catalytic performance of Bi_2O_3-ZnO/bentonite clay.

Enhanced visible light-harvesting capacity, avoided recombination, and enhanced adsorption–photodegradation activity in multidimensional TiO_2-BiOBr- bentonite ternary heterostructures were observed at the ternary heterojunction between TiO_2 and BiOBr and bentonite (Figure 14) [118]. The composite's excellent light-harvesting capacity, good charge

transfer efficiency, and high Brunauer–Emmett–Teller (BET) surface area are responsible for its increased photocatalytic activity toward phenol under visible light irradiation, as compared to pure anatase- TiO_2 and BiOBr.

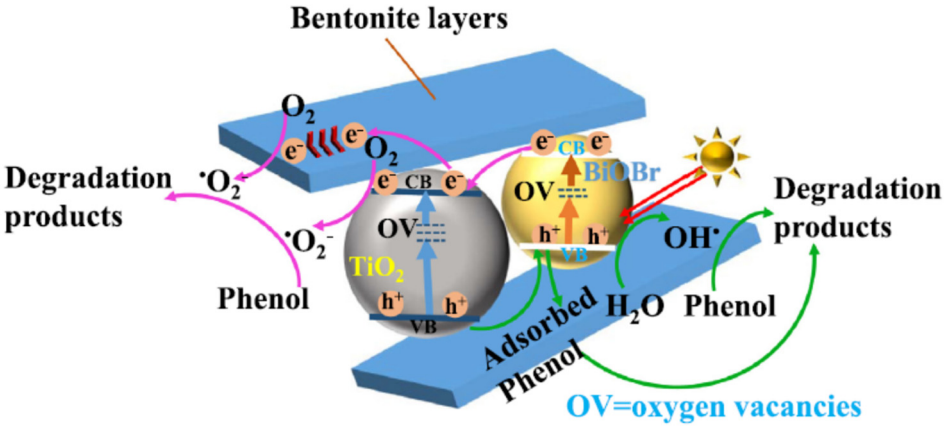


Figure 14. Charge transfer mechanism for the degradation of phenol on TiO_2-BiOBr- bentonite ternary heterostructures. Reproduced with permission [118].

The immobilization of BiOCl/ZnO on the bentonite surface was reported by Vaizoğullar et al. [119]. Bentonite was included in the as-made composite to raise its BET surface area. The composite catalysts displayed increased photoactivity under UV radiations, which may be related to the effective reduction in the recombination rate of charge carriers, as shown by the observed photocatalytic performance of the produced catalysts.

2.3.3. Bismuth-Based Photocatalysts/Sepiolite

Due to its molecular-sized channels and rich hydroxyl groups, natural sepiolite, which belongs to the 2:1 class of clay minerals, has garnered a lot of attention in recent years from a variety of industries. In light of its low cost, high mechanical and chemical durability, and high adsorption capability, sepiolite is widely considered to be an ideal catalytic support material. Example: using a straightforward hydrolysis precipitation–calcination crystallization approach followed by the solvothermal method, researchers were able to create unique ternary Bi_2MoO_6/TiO_2/sepiolite photocatalysts [120]. The ternary hierarchical composite was formed by coupling sepiolite and Bi_2MoO_6/TiO_2, which was mostly responsible for the vastly increased photodegradation performance of HCHO for the composite. The separation efficiency of photoinduced carriers may be raised, the visible light-response capability can be boosted, and the adsorption capacity can be increased using such a structure (Figure 15). Thanks to its ability to evenly disperse TiO_2 and Bi_2MoO_6, sepiolite contributes favorably to the development of ternary hierarchical composite.

It was also shown that $BiVO_4$/sepiolite nanocomposites could be made using the hydrothermal method [121]. The produced nanocomposites showed strong bonding at the $BiVO_4$/sepiolite interface, which improved the separation of photogeneration carriers and resulted in an outstanding performance of TC and MB photocatalytic degradation under visible light irradiation.

2.3.4. Bismuth-Based Photocatalysts/Rectorite

Composites were constructed using a variety of clays, including those mentioned above and others found to have properties conducive to boosting photocatalytic activity. Ultrasound-assisted synthesis was utilized to mix Bi_2NbO_5F with rectorite clay, which consists of alternating pairs of the nonexpandable dioctahedral mica-like layer and expandable dioctahedral smectite layer in the ratio of 1:1, for the degradation of RhB [122]. When tested against a bare Bi_2NbO_5F sample, the composite containing 32% rectorite showed 6.6 times the photocatalytic degradation efficiency in decomposing RhB in an aqueous solution. The high adsorbability and higher light absorption of the composite are likely responsible for its

improved activity. Rectorite in the composite photocatalyst serves to segregate the electrons and holes and reduce charge recombination, resulting in more active sites for adsorption and photocatalytic activity.

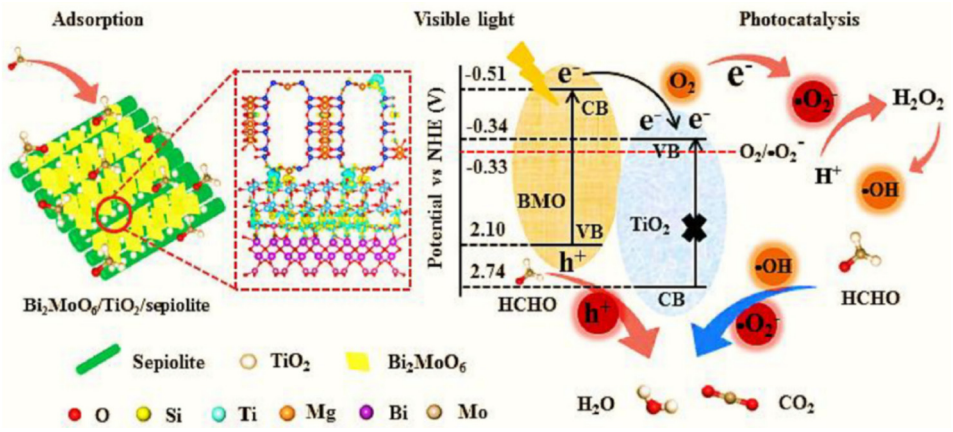


Figure 15. The potential photocatalytic mechanism for HCHO removal under visible light by Bi_2MoO_6/TiO_2/sepiolite composite. Reproduced with permission [120].

2.3.5. Bismuth-Based Photocatalysts/Saponite

Hydrothermally prepared tertiary composites of BiOBr, carbon quantum dots (CQDs), and the smectite group mineral saponite were employed for ciprofloxacin degradation [123]. The enhanced interaction between BiOBr and CQDs was a result of the stronger interaction of CQDs and better distribution of CQDs on the surface of saponite, which prevented the reagglomeration of excess CQDs on the surface of BiOBr and, thus, preserved the amount of active surface available to receive the light and react with CIP.

2.3.6. Bismuth-Based Photocatalysts/Palygorskite

The clay mineral palygorskite has a microfibrous shape, a low surface charge, a high magnesium concentration, and a high specific surface area. According to a study by Luo et al., the microspheres composite may be created using a simple coprecipitation and calcination approach by introducing protonated palygorskite nanofibers (Pal) into Bi_5O_7I nanosheets (Figure 16a) [124]. Photocatalytic degradation of tetracycline hydrochloride (TCH) and CIP was enhanced by a combination of factors including a tight contact interface, hierarchical structure, enhanced optical response capability, and an S-scheme heterojunction. In addition, during solar light irradiation, the palygorskite played a critical function in the system by increasing the specific surface area, speeding up the charge separation, and decreasing the length of the charge transfer channel (Figure 16b).

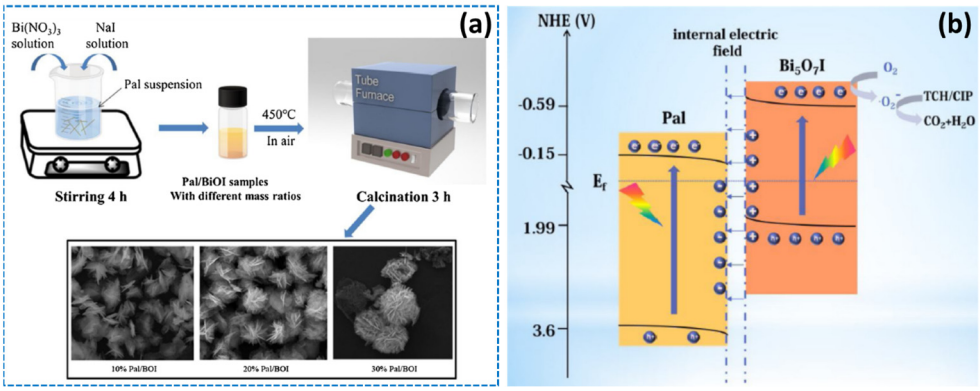


Figure 16. (**a**) Preparation of series of Bi_5O_7I/palygorskite heterojunction photocatalysts and (**b**) photocatalytic mechanisms of the Bi_5O_7I/palygorskite composite for TCH and CIP degradation. Reproduced with permission [124].

2.3.7. Bismuth-Based Photocatalysts/Laponite

For its large surface area and cation-exchange capability, laponite is a readily modifiable magnesiosilicate smectite clay with dimensions of 25 nm in diameter and 0.92 nm in thickness. The BiOI's crystalline development was reportedly stifled by a nanoscopic layered silicate laponite template, resulting in smaller particles, different surface chemistry, and better water dispersibility, as reported by Liu et al. [125]. Photogenerated charge separation along the axis of the internal electric field of BiOI was facilitated by the smaller particle size and the prominent 001 facets, resulting in an increase in the efficiency for MO degradation. Thus, the use of such clay in conjunction with bismuth-based photocatalysts holds great promise for both the synthesis of composite photocatalysts and the purification of polluted environments.

2.4. Other Photocatalysts/Clay Composites

2.4.1. Plasmonic Nanoparticles Incorporated in Clay-Based Photocatalysts

Over the past several years, the introduction of noble metallic nanoparticles (e.g., Au, Ag, and Pt, etc.) into the photocatalysts for an improvement in their photocatalytic performance has intensively gained attention from research communities due to the strong SPR of the plasmonic metal nanoparticles, which may improve visible light absorption [126]. Generally, the SPR is a physical phenomenon that happens when free electrons oscillate with incident photons confined on the surface of the noble metallic nanoparticles (Figure 17). The enhancement in photocatalytic activity in SPR-mediated photocatalytic materials can be caused by the photoinduced electrons rapidly migrating from noble metallic nanoparticles to the conduction band of the semiconductors because the Schottky barriers can be formed at the plasmonic metal–semiconductor interface, while the holes still remain in the valence band [127]. Thus, the charge carrier recombination from the excitation sites in both the semiconductors and noble metal nanoparticles could be mitigated (Figure 18) [128]. Recent publications on the decoration of plasmonic nanoparticles into clay-based photocatalysts and their application for the environmental decontamination of wastewater will be discussed.

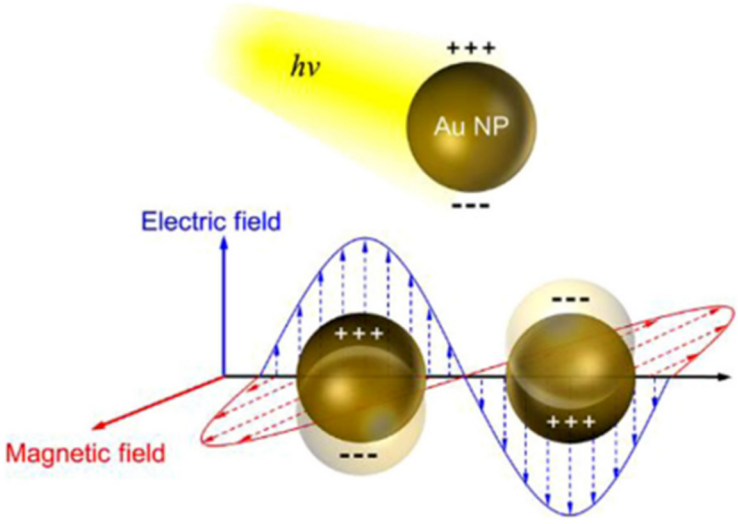


Figure 17. Schematic illustration of the surface plasmon resonance (SPR) excitation of noble metallic nanoparticles. Reproduced with permission [126].

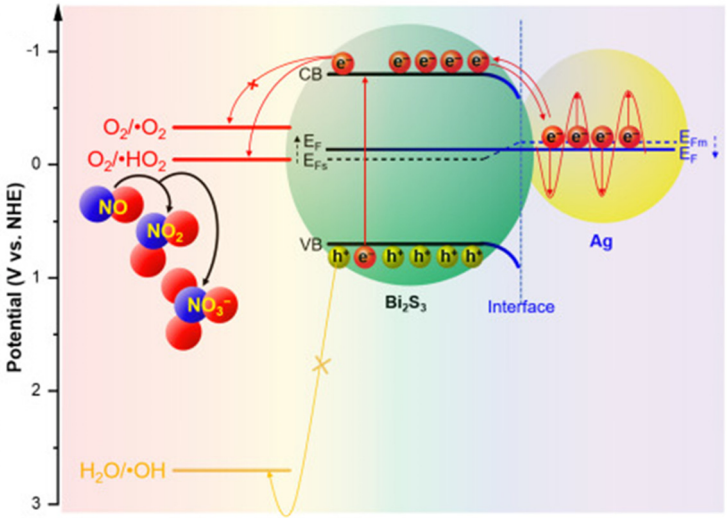


Figure 18. Possible migration of photogenerated electrons in the SPR-enhanced photocatalysis of Ag nanoparticle-decorated Bi_2S_3 for NO degradation. Reproduced with permission [128].

Mishra et al. prepared the composite materials between bentonite clay and plasmonic metallic nanoparticle-loaded TiO_2 by varying the different types of the noble metals (Ag, Au, and Pd) by the chemical reduction–precipitation method [129]. The SPR induced by the noble metallic nanoparticles could enable the significant suppression of the electron–hole pair recombination and effectively enhance the photocatalytic degradation of toxic volatile organic compounds (400-ppm chlorobenzene and 10-ppm benzaldehyde) in water under UV and visible light irradiation. Interestingly, the Ag nanoparticle-loaded composite demonstrated the highest photocatalytic performance for the degradation of chlorobenzene (99% under UV for 30 min, 88% under visible light for 60 min) and benzaldehyde (96% under UV for 70 min, 78% under visible light for 160 min) due to a higher exciton lifetime (suggested by the time-resolved fluorescence spectroscopy). Moreover, after the introduction of noble metals into the composites, the porosity and specific surface area of the composites were slightly increased (about 5%) because of the small size of the deposited metal (18–10 nm) impregnation, which feasibly increased the photocatalytic performance. Similarly, the composite material between Au nanoparticle-modified N and S-doped TiO_2 with kaolinite clay was synthesized by the sol-gel method, followed by an oxalic reduction for Au deposition [130]. The as-obtained composite was further used as a photocatalyst for the degradation of methylene blue aqueous solution (2.5 mM) under direct sunlight illumination. Obviously, the rate constant for the photocatalytic degradation of methylene blue dye was improved by 82% after the Au nanoparticles loading compared to that of the unloaded kaolinite/TiO_2 composites. The enhancement in photocatalytic activity in Au-loaded kaolinite/TiO_2 is possibly caused by the electromagnetic field amplification from the SPR. In addition, Ag-Bi_2O_3/montmorillonite was prepared by a simple thermal and wet impregnation method, followed by the ascorbic acid reduction in Ag^+ and utilized as a photocatalyst for the remediation of wastewater contaminated with TC under visible light [112]. The SPR of the Ag nanoparticles impressively avoided the electron–hole pair recombination and improved the visible light adsorption, resulting in an enhancement in the photocatalytic performance in the TC degradation from 65% (for Bi_2O_3/montmorillonite) to 90% (for Ag-Bi_2O_3/montmorillonite).

As mentioned in the previous works, the plasmonic noble metal nanoparticles were usually deposited on semiconductors/clay composite materials. Alternately, the plasmonic nanoparticles can be incorporated in semiconducting clays such as LDH which has been considered a promising photocatalyst to replace the conventional TiO_2 [127]. However, there are two main limitations of using LDH as efficient photocatalysts, which are the ability of UV-visible light adsorption and the fast charge carrier recombination. Thus, the deposition of plasmonic nanoparticles in LDH-based photocatalysts could alleviate

the aforementioned problems. For example, a Mg-Al LDH photocatalyst decorated with different plasmonic metals (Cu, Ag, and Au, 1–3 wt%) was synthesized by a solvothermal method followed by photochemical deposition and further applied for the photocatalytic decomposition of tetracycline (50 ppm) under LED light. The order of the photocatalytic activity trend for the TC degradation was Au@LDH (99%) > Ag@LDH (94%) > Cu@LDH (74%) > pristine LDH (23%), confirming that the SPR from the plasmonic nanoparticles can greatly improve the photocatalytic activity due to the high response in the visible light region and effective charge separation [131]. Traditionally, the deposition of plasmonic metals on metal–semiconductor composites has been conducted using the soluble salts of plasmonic metals and reducing agents. This approach can cause serious concern about the toxicity of metal soluble salts and the secondary pollution risk. Thus, an alternative method using mechanochemical methods to reduce the metal ion to metallic nanoparticles has been considered a simple and green approach. In 2018, a plasmonic Ag/Zn–Al LDH photocatalyst was successfully fabricated by cogrinding $AgNO_3$ with Zn–Al LDH raw materials. Interestingly, the reduction in $AgNO_3$ to Ag metallic nanoparticles in this work was carried out using ball-milling mixing [127]. After the preparation of the Ag/Zn–Al LDH composites, the as-obtained material was employed for the photocatalytic remediation of water contaminated with methyl orange (100 ppm) under visible light irradiation. The experimental results implied that the Schottky barrier at the interface between Ag and Zn–Al LDH and the SPR effect significantly enhanced the photocatalytic degradation of methyl orange about five times greater than that of the pristine LDH sample. Furthermore, another approach to obtain high-performance photocatalysts for wastewater remediation by SPR-mediated clay composites is the incorporation of the plasmonic metals into the semiconducting materials and, consequently, the construction of the composites between them and the LDHs. Reported by Tonda et al. [132], a Ag nanoparticle-decorated NiAl-layered double hydroxide/graphitic carbon nitride (Ag/LDH/g-C_3N_4) composite demonstrated dramatically high photocatalytic activity toward the degradation of aqueous RhB (5 ppm) and 4-chlorophenol (5 ppm) solutions under visible light illumination. The Ag-loaded LDH/g-C_3N_4 photocatalyst showed a greater photocatalytic degradation of RhB and 4-chlorophenol of 1.6 and 1.8 times that of the unloaded LDH/g-C_3N_4 composite. Similarly, the Pd-Fe_3O_4/NiFe-LDH composites exhibited a higher efficiency (96%) in the photocatalytic degradation of metoclopramide (20 ppm) under visible light than those of the pure NiFe-LDH (38%) or Fe_3O_4/NiFe-LDH (62%). Interestingly, the superparamagnetic behavior of the Pd-Fe_3O_4/NiFe-LDH composite, which can be magnetically separated from the aqueous media, allowed the easy separation process for the recovery of the photocatalysts with the assistance of the applied external magnetic field after utilization [133].

2.4.2. Modification of Clay-Based Photocatalysts with Metal–Organic Frameworks (MOFs), Mxene, Black Phosphorus, and Quantum Dots

Composites of metal–organic frameworks (MOFs) and clay materials have been considered as a relatively new research avenue in the photocatalytic remediation of contaminated aqueous solutions. The benefits of coupling clay with MOFs are to solve the instability problem of MOFs and reduce production costs [134]. Importantly, the heterojunction at the interface of MOF–clay composites can strongly mitigate the charge carrier recombination process, resulting in enhancing the photocatalytic activity. A recent report by Pawar et al. showed the application of a natural sepiolite clay composited with MOFs ($Zr_6O_4(OH)_4$(2-aminobenzene-1,4-dicarboxylic acid)$_6$) as a photocatalyst for the degradation of RhB aqueous solution under visible light [134]. The introduction of sepiolite in the MOFs@sepiolite composite can not only improve the photocatalytic activity but also increase the specific surface area and thermal stability. The MOFs@sepiolite photocatalyst showed a higher RhB photocatalytic degradation (~88%) than that of the pure MOFs (~18%) and pristine sepiolite (~70%). Additionally, a ZnMgAl-layered triple hydroxide (ZnMgAl LTH)/MOFs-5 composite was prepared by Bhuvaneswari et al. and further applied as a photocatalyst to remediate water contamination with MB under UV-visible

light irradiation [135]. The ZnMgAl LTH/MOFs-5 displayed a photocatalytic activity (98%) nearly two times greater than those of the ZnMgAl LTH (43%) and MOFs-5 (58%) due to the enhanced visible light-adsorption capability, effective charge separation, and charge transportation during the photocatalytic process. The as-synthesized composite exhibited a high stability, maintaining its initial photocatalytic efficiency with no significant loss for five cycles. Similarly, Ti-MOFs/Ag/NiFeLDH composites were fabricated with the concept of utilizing the unique properties of MOFs, Ag plasmonic nanoparticles, and NiFeLDH semiconducting clays to obtain a high-permeance photocatalyst for RhB and levofloxacin (LVX) degradation in water under visible light [136]. The Ti-MOFs/Ag/NiFeLDH composites demonstrated excellent photocatalytic activities for 95% RhB degradation and 92% LVX decomposition within 50 min and 70 min, respectively. The boosted photocatalytic activity in the Ti-MOFs/Ag/NiFeLDH composites is caused by the effective suppression of the charge recombination and the transportation of the photoinduced electrons and holes by the SPR and heterojunction of the Ti-MOFs/NiFeLDH.

Recently, composites between LDH and $Ti_3C_2T_xC$ (MXene) for photocatalytic application in wastewater treatment have been reported but there is a limited number of publications. Previously, LDH/Mxene composites were mainly applied as adsorbents, supercapacitors, sensors, and catalysts in oxygen evolution reactions. It is expected that Mxene compounds are a promising candidate to replace the noble metal as cocatalysts in the photocatalytic process. In 2021, a 3D marigold-like CoAl-LDH/Mxene composite was prepared by Wang et al. and employed as a photocatalyst for the degradation of 25-ppm antibiotic aqueous solutions (tetracycline hydrochloride, chloramphenicol, and terramycin) under visible light [137]. The CoAl-LDH/Mxene composite exhibited an improvement of 3.1, 3.0, and 2.1 times that of the degradation efficiency of tetracycline hydrochloride (85%), chloramphenicol (56%), and terramycin (70%), respectively, higher than those of the pristine CoAl-LDH. The presence of Mxene affected the morphology evolution from the 2D nanoplate to the 3D hierarchical architecture of the CoAl-LDH/Mxene composite, subsequently enhancing the adsorption capacity and proton capture of the materials. Moreover, an impressive electron transfer from CoAl-LDH to Mxene would be promoted due to the well-defined 2D/2D interface, resulting in the effective suppression of the recombination of the photogenerated electron–hole pairs on the CoAl-LDH. Additionally, 2D/2D NiFe-LDH/MXene and Zn/Ti-LDH/MXene composites were also synthesized and consequently served as efficient photocatalysts for water treatment applications. The 2D/2D NiFe-LDH/MXene demonstrated 3.8-fold enhanced degradation kinetics of norfloxacin under simulated sunlight irradiation compared to that of the bare NiFe-LDH [138]. Moreover, the Zn/Ti-LDH/MXene composites delivered a superior photocatalytic degradation of acetaminophen (100% within 40 min) and ibuprofen (99.7% within 60 min) under simulated solar light [139]. Similarly, the existence of MXene in the structure of the composites can promote electron transport, avoiding the photogenerated electron–hole pair recombination; thus, the photocatalytic activity in the materials can be enhanced (Figure 19).

Another choice of semiconducting materials to fabricate the composite with clays for photocatalytic application is black phosphorus nanosheets (BPN), which are a 2D-semiconductor with a broad spectral response from UV to the NIR light region. Moreover, it is expected that the heterojunction of LDH clays and BPN can also improve the separation efficiency of photogenerated charges, resulting in enhancing the photocatalytic activity in the materials. In 2021, a BPN composited with ZnAl-LDH was prepared and used as a highly efficient and nontoxic photocatalyst for the decomposition of MB aqueous solution under visible light. The BPN/ZnAl-LDH composite showed a higher photocatalytic degradation efficiency (99%) than those of the pure BPN (11%) and pristine ZnAl-LDH (63%). The enhancement in the photocatalytic performance in the BPN/ZnAl-LDH composite was due to the effective electron transfer from the ZnAl-LDH component to BPNs [140].

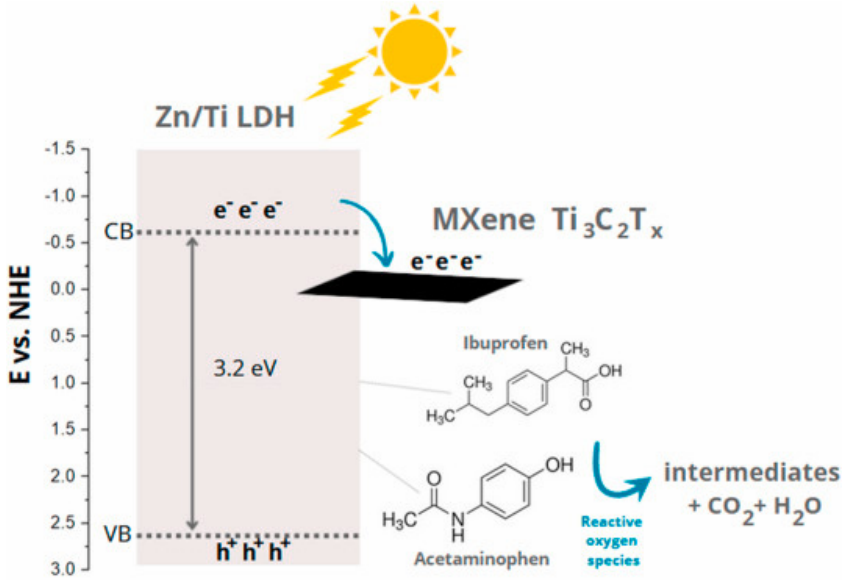


Figure 19. Schematic illustration of possible transportation of photogenerated electrons in the Zn/Ti-LDH/MXene composites for acetaminophen and ibuprofen degradation. Reproduced with permission [139].

As a cocatalyst, quantum dots (QDs) are nanomaterials that are based on carbon and have been produced recently. CDs are characterized by their small size and high specific surface area, which enables them to provide a large number of sites for surface adsorption and surface contracting with the primary photocatalyst. Because CDs already have a sizeable number of hydrophilic functional moieties, it is not necessary to make any further modifications in order to provide them with the hydrophilic properties and reactive capacities associated with those qualities. Therefore, the absorption and surface properties of CDs are greatly impacted by parameters such as the size of the conjugated domains, fluctuations in the oxygen and nitrogen content of the carbon cores, the types of surface groups, and the number of surface groups that are present. Therefore, the creation of CDs and their composites might potentially be used as alternative adsorbents for the treatment of wastewater. Similar to other photocatalytic material works, the decoration of QDs to alleviate the light adsorption and electron–hole pair recombination issues in clay-based photocatalysts was also reported by Amani-Ghadim et al. in 2019. The ZnS quantum dots composited with a MnZnAl-LDH photocatalyst were used for the efficient photocatalytic degradation of acid red 14 (500 ppm) in water under visible light. The much superior photocatalytic efficiency in acid red 14 degradation catalyzed by MnZnAl-LDH/ZnS QDs (85%) to pure ZnS QDs (<10%) was observed [141]. Similarly, the CdTe QDs incorporated in CoNiAl-LDH as a highly visible light-responsive photocatalyst for the degradation of acid red 14 (AR14, 20 ppm) and bisphenol A (BPA, 5 ppm) in water was also reported in 2022 [142]. About 96% AR14 (120 min) and 80% BPA (within 180 min) photocatalytic degradation efficiencies were accomplished by using the CdTe QDs-CoNiAl-LDH photocatalyst while much smaller efficiencies from the pristine CoNiAl-LDH (~25% for AR14 and 19% for BPA) and pure CdTe QDs (~38% for AR14 and ~20% for BPA) were obtained. The improvement in photocatalytic efficiency may be attributed to the enhanced light-harvesting ability in the visible region and effective suppression of the charge carrier recombination after the introduction of the QDs into the structure of the composite materials. In certain water treatment applications, hydrogels have been used; nevertheless, the efficiency and strength of these hydrogels are insufficient to warrant their general use. Recently, hydrogel-clay nanocomposites have been presented as a solution to the inherent difficulties that are encountered when using hydrogels for water purification. Some hydrogel nanocomposites are prepared with clay and used for bactericidal application. For example, the use of an in situ nanoclay-reinforced free radical gelation approach, a

robust hydrogel containing Ag nanoparticles, has been produced and used as the catalyst for the conversion of the 4-nitrophenol and inhibition zones of *E. coli* [143]. Because of their high porosity and specific surface area, hydrogel nanocomposites make excellent photocatalysts. This is because they have a large number of active sites that are accessible for the adsorption of reactants. However, clay-based hydrogel nanocomposites have only been investigated for their adsorption capabilities. Because of this, their potential as photocatalysts has not yet been fully investigated.

Based on the above discussion, the comparison table between several clay-based photocatalysts for wastewater remediation is summarized as shown in Table 1. It can be seen that the two-dimensional clay-based composite, such as montmorillonite, showed a higher photocatalytic performance than the one-dimensional pillar clay, such as a sepiolite, due to a higher contract area via the heterojunction in the composite. Moreover, the clay-based photocatalyst showed a high stability and reusability in several reports because clay has a high stability in a wide range of photocatalytic conditions such as temperature and pH. In addition, the photocatalytic processing, including the effectiveness of photocatalysts, the deactivation, and regeneration phases, as well as the answers to identified technical challenges, should be evaluated in actual settings in order to improve photocatalytic technology investment and transfer to practical application. Sustainability, the cost of developing novel photocatalytic materials, and the cost of ownership of photocatalytic systems are all important factors that need to be taken into consideration. In comparison to the commercially available TiO_2 and TiO_2-clay composites, the clay-based photocatalyst could provide not only a higher photocatalytic activity for wastewater remediation, but it can also reduce the cost of the utilizing material. By the same token, clay, which normally has a low cost and is an earth-abundant material, could reduce the utilization of the main TiO_2 which has a higher price compared with clay. Thus, the clay-based photocatalyst could bring the photocatalytic process for wastewater treatment to practical application with cost-effectiveness.

Table 1. Photocatalytic treatment of organic/inorganic contamination using clay-based composites.

Pollutant	Photocatalyst	Clay	Efficiency	Time	Ref.
2-mercaptobenzothiazole	Fe_3O_4@g-C_3N_4/ATP	attapulgite	90%	90 min	[72]
ciprofoxacin	Sepiolite/g-C_3N_4	sepiolite	90%	60 min	[82]
methylene blue	TiO_2/montmorillonite	montmorillonite	98%	90 min	[88]
$Cr^{(VI)}$	TiO_2/kaolin	kaolin	98%	120 min	[92]
2,4-dichlorophenol	TiO_2/sepiolite	sepiolite	90%	120 min	[104]
$Cr^{(VI)}$	TiO_2/bentonite	bentonite	100%	180 min	[98]
tetracycline	Ag-loaded Bi_2O_3/montmorillonite	montmorillonite	100%	45 min	[112]
rhodamine B	BiOBr/Na-montmorillonite	montmorillonite	100%	60 min	[113]
rhodamine B	BiOCl/montmorillonite	montmorillonite	100%	30 min	[115]
formaldehyde	Bi_2MoO_6/TiO_2/sepiolite	sepiolite	100%	195 min	[120]
methylene blue	$BiVO_4$/sepiolite	sepiolite	90%	150 min	[121]
ciprofoxacin	BiOBr/saponite/CQD	saponite	100%	5 min	[123]
ciprofoxacin	Bi_5O_7I/palygorskite	palygorskite	100%	80 min	[124]
rhodamine B	Pd-Fe_3O_4/NiFe-LDH	NiFe-LDH	96%	30 min	[133]
rhodamine B	MOFs@sepiolite	sepiolite	88%	120 min	[134]

3. Conclusions

This article provided an overview of clay-based photocatalysts, such as TiO_2, g-C_3N_4, and Bi-based compounds, and others, for the degradation of organic contaminants in wastewater. Clay minerals with high specific surface areas, high adsorption capacity, large pore volumes, chemical stability, and good mechanical properties enhance the decomposition of organic pollutants by photocatalytic degradation when present in composites, so this area of study has been expanding rapidly in recent years. Different kinds of photocatalysts were supported using clay minerals. Dispersing photocatalyst nanoparticles onto the surfaces of clay minerals enhances the photocatalytic activity in photocatalysts

by increasing the number of active surface sites and decreasing particle aggregation. It has been discovered that clays tend to increase the photocatalytic activity in nanoparticle photocatalysts. Thus, more active surface sites are provided by clay during the synthesis of clay-based composites, aggregation of the primary photocatalyst particles is prevented, and nanoparticle release is inhibited. In certain instances, clay also helps with the generation of active radicals for the breakdown of organic contaminants by facilitating the separation of photogenerated electrons and holes. Some impurities in the clay, such as Fe, may improve the optical characteristics of clay and modify its photoresponse activity. For instance, when montmorillonite had some Fe impurity, the job of this clay in the photocatalyst composite was not only to offer the site for the formation of the primary photocatalyst but also to engage in the electron transfer mechanism to avoid charge carrier recombination. Furthermore, surface contact between the clay and the primary photocatalyst is essential for wastewater treatment. The large surface area of clay, such as a two-dimensional or sheet-like structure clay such as montmorillonite, may provide more surface interaction between the clay and the main photocatalyst than a one-dimensional or pillar-like structure clay such as attapulgite and sepiolite, thereby enhancing the separation of the electrons and holes in the main photocatalyst. Therefore, the clay in clay-based photocatalysts not only acts as a template to prevent the agglomeration and development of the major photocatalysts but also provides the considerable suppression of charge recombination, which may prolong the lifetime of the electron–hole pair and enhance the degrading activity. This study proves that the composite of clay minerals used to create photocatalysts has great promise for use in low-cost, solar-powered environmental remediation.

Author Contributions: Writing original draft preparation: C.C., J.T., K.S. (Kaiqian Shu), L.Z., S.S., A.S., S.M. and K.S. (Karthikeyan Sekara); review and editing: C.C.; writing, review and editing: C.C.; conceptualization, supervision, and project administration: C.C.; funding acquisition: C.C. and K.S. (Keiko Sasaki). All authors have read and agreed to the published version of the manuscript.

Funding: The work was supported by the Japan Society for the Promotion of Science (JSPS) KAKENHI (A) [No. JSPS JP22H00266]. This work was partly supported by the Advanced Research Infrastructure for Materials and Nanotechnology Grant Number JPMXP1222KU1009 in Japan sponsored by the Ministry of Education, Culture, Sports, Science and Technology (MEXT), Japan. This work was partly supported by the 2022 Research Start Program 202208 to Chitiphon Chuaicham.

Data Availability Statement: Not applicable.

Conflicts of Interest: The authors declare no conflict of interest.

References

1. Srikhaow, A.; Smith, S.M.; Uraisin, K.; Suttiponparnit, K.; Kongmark, C.; Chuaicham, C. Catalytic remediation of phenol contaminated wastewater using Cu-Zn hydroxide nitrate. *RSC Adv.* **2016**, *6*, 36766–36774. [CrossRef]
2. Tian, Q.; Guo, B.; Chuaicham, C.; Sasaki, K. Mechanism analysis of selenium (VI) immobilization using alkaline-earth metal oxides and ferrous salt. *Chemosphere* **2020**, *248*, 126123. [CrossRef]
3. Prabhu, S.M.; Chuaicham, C.; Park, C.M.; Jeon, B.H.; Sasaki, K. Synthesis and characterization of defective UiO-66 for efficient co-immobilization of arseate and fluoride from single/binary solutions. *Environ. Pollut.* **2021**, *278*, 116841. [CrossRef]
4. Higashimoto, S.; Kurikawa, Y.; Tanabe, Y.; Fukushima, T.; Harada, A.; Murata, M.; Sakata, Y.; Kobayashi, H. Photocatalytic property of WO_3 modified with noble metal co-catalysts towards selective hydroxylation of benzene to phenol under visible light irradiation. *Appl. Catal. B Environ.* **2023**, *325*, 122289. [CrossRef]
5. Chen, X.; Wang, Z.; Shen, X.; Zhang, Y.; Lou, Y.; Pan, C.; Zhu, Y.; Xu, J. A plasmonic Z-scheme Ag@AgCl/PDI photocatalyst for the efficient elimination of organic pollutants, antibiotic resistant bacteria and antibiotic resistance genes. *Appl. Catal. B Environ.* **2023**, *324*, 122220. [CrossRef]
6. Ning, L.; Chen, X.; Wang, Z.; Xu, J. High-efficiency pollutant degradation, disinfection and H_2O_2 production activities of magnetically separable Co-imbedded N-doped carbonaceous framework/supramolecular perylene diimide photocatalyst. *Appl. Catal. B Environ.* **2023**, *324*, 122282. [CrossRef]
7. Mishra, A.; Mehta, A.; Basu, S. Clay supported TiO_2 nanoparticles for photocatalytic degradation of environmental pollutants: A review. *J. Environ. Chem. Eng.* **2018**, *6*, 6088–6107. [CrossRef]
8. Balakumar, V.; Manivannan, R.; Chuaicham, C.; Karthikeyan, S.; Sasaki, K. A simple tactic synthesis of hollow porous graphitic carbon nitride with significantly enhanced photocatalytic performance. *Chem. Commun.* **2021**, *57*, 6772–6775. [CrossRef]

9. Chen, X.; Shen, S.; Guo, L.; Mao, S.S. Semiconductor-based Photocatalytic Hydrogen Generation. *Chem. Rev.* **2010**, *110*, 6503–6570. [CrossRef]
10. Ni, M.; Leung, M.K.H.; Leung, D.Y.C.; Sumathy, K. A review and recent developments in photocatalytic water-splitting using TiO_2 for hydrogen production. *Renew. Sustain. Energy Rev.* **2007**, *11*, 401–425. [CrossRef]
11. Zhao, X.; Xu, M.; Song, X.; Zhou, W.; Liu, X.; Yan, Y.; Huo, P. Charge separation and transfer activated by covalent bond in UiO-66-NH_2/RGO heterostructure for CO_2 photoreduction. *Chem. Eng. J.* **2022**, *437*, 135210. [CrossRef]
12. Balu, S.; Chuaicham, C.; Balakumar, V.; Rajendran, S.; Sasaki, K.; Sekar, K.; Maruthapillai, A. Recent development on core-shell photo(electro)catalysts for elimination of organic compounds from pharmaceutical wastewater. *Chemosphere* **2022**, *298*, 134311. [CrossRef]
13. Xiang, Q.; Cheng, B.; Yu, J. Graphene-Based Photocatalysts for Solar-Fuel Generation. *Angew. Chem. Int. Ed.* **2015**, *54*, 11350–11366. [CrossRef]
14. Shearer, C.J.; Cherevan, A.; Eder, D. Application and Future Challenges of Functional Nanocarbon Hybrids. *Adv. Mater.* **2014**, *26*, 2295–2318. [CrossRef]
15. Chuaicham, C.; Sekar, K.; Balakumar, V.; Mittraphab, Y.; Shimizu, K.; Ohtani, B.; Sasaki, K. Fabrication of graphitic carbon nitride/ZnTi-mixed metal oxide heterostructure: Robust photocatalytic decomposition of ciprofloxacin. *J. Alloys Compd.* **2022**, *906*, 164294. [CrossRef]
16. Long, Z.; Li, Q.; Wei, T.; Zhang, G.; Ren, Z. Historical development and prospects of photocatalysts for pollutant removal in water. *J. Hazard. Mater.* **2020**, *395*, 122599. [CrossRef]
17. Tong, H.; Ouyang, S.; Bi, Y.; Umezawa, N.; Oshikiri, M.; Ye, J. Nano-photocatalytic Materials: Possibilities and Challenges. *Adv. Mater.* **2012**, *24*, 229–251. [CrossRef]
18. Chuaicham, C.; Inoue, T.; Balakumar, V.; Tian, Q.; Ohtani, B.; Sasaki, K. Visible light-driven ZnCr double layer oxide photocatalyst composites with fly ashes for the degradation of ciprofloxacin. *J. Environ. Chem. Eng.* **2022**, *10*, 106970. [CrossRef]
19. Okab, A.A.; Alwared, A.I. Photodegradation of tetracycline antibiotic by ternary recyclable Z-scheme g-C_3N_4/Fe_3O_4/Bi_2WO_6/Bi_2S_3 photocatalyst with improved charge separation efficiency: Characterization and mechanism studies. *Environ. Nanotechnol. Monit. Manag.* **2023**, *19*, 100767. [CrossRef]
20. Mehta, A.; Mishra, A.; Sharma, M.; Singh, S.; Basu, S. Effect of silica/titania ratio on enhanced photooxidation of industrial hazardous materials by microwave treated mesoporous SBA-15/TiO_2 nanocomposites. *J. Nanoparticle Res.* **2016**, *18*, 209. [CrossRef]
21. Asiltürk, M.; Şener, Ş. TiO_2-activated carbon photocatalysts: Preparation, characterization and photocatalytic activities. *Chem. Eng. J.* **2012**, *180*, 354–363. [CrossRef]
22. Chong, M.N.; Tneu, Z.Y.; Poh, P.E.; Jin, B.; Aryal, R. Synthesis, characterisation and application of TiO_2–zeolite nanocomposites for the advanced treatment of industrial dye wastewater. *J. Taiwan Inst. Chem. Eng.* **2015**, *50*, 288–296. [CrossRef]
23. Szczepanik, B. Photocatalytic degradation of organic contaminants over clay-TiO_2 nanocomposites: A review. *Appl. Clay Sci.* **2017**, *141*, 227–239. [CrossRef]
24. Liu, J.; Zhang, G. Recent advances in synthesis and applications of clay-based photocatalysts: A review. *Phys. Chem. Chem. Phys.* **2014**, *16*, 8178–8192. [CrossRef]
25. Papoulis, D.; Komarneni, S.; Panagiotaras, D.; Nikolopoulou, A.; Christoforidis, K.C.; Fernández-Garcia, M.; Li, H.; Shu, Y.; Sato, T. Palygorskite–TiO_2 nanocomposites: Part 2. photocatalytic activities in decomposing air and organic pollutants. *Appl. Clay Sci.* **2013**, *83–84*, 198–202. [CrossRef]
26. Neeraj, K.; Chandra, M. Basics of Clay Minerals and Their Characteristic Properties. In *Clay and Clay Minerals*; Gustavo Morari Do, N., Ed.; IntechOpen: Rijeka, Croatia, 2021; Chapter 2. [CrossRef]
27. Praise, A. Classification of Clay Minerals. In *Mineralogy*; Miloš, R., Ed.; IntechOpen: Rijeka, Croatia, 2022; Chapter 12. [CrossRef]
28. Hartati; Prasetyoko, D.; Santoso, M.; Qoniah, I.; Leaw, W.L.; Firda, P.B.D.; Nur, H. A review on synthesis of kaolin-based zeolite and the effect of impurities. *J. Chin. Chem. Soc.* **2020**, *67*, 911–936. [CrossRef]
29. Massaro, M.; Noto, R.; Riela, S. Past, Present and Future Perspectives on Halloysite Clay Minerals. *Molecules* **2020**, *25*, 4863. [CrossRef]
30. Khalifa, A.Z.; Cizer, Ö.; Pontikes, Y.; Heath, A.; Patureau, P.; Bernal, S.A.; Marsh, A.T.M. Advances in alkali-activation of clay minerals. *Cem. Concr. Res.* **2020**, *132*, 106050. [CrossRef]
31. Zou, Y.; Hu, Y.; Shen, Z.; Yao, L.; Tang, D.; Zhang, S.; Wang, S.; Hu, B.; Zhao, G.; Wang, X. Application of aluminosilicate clay mineral-based composites in photocatalysis. *J. Environ. Sci.* **2022**, *115*, 190–214. [CrossRef]
32. Mohamed, A. Effect of potassium saturation on the mineralogical composition and ceramic properties of smectitic clays from the Eastern Desert, Egypt. *J. African Earth Sci.* **2021**, *176*, 104139. [CrossRef]
33. Bourdelle, F. Low-Temperature Chlorite Geothermometry and Related Recent Analytical Advances: A Review. *Minerals* **2021**, *11*, 130. [CrossRef]
34. Franco, J.G.; Ataide, J.A.; Ferreira, A.H.P.; Mazzola, P.G. Lamellar compounds intercalated with anions with solar protection function: A review. *J. Drug Deliv. Sci. Technol.* **2020**, *59*, 101869. [CrossRef]
35. Zubair, M.; Daud, M.; McKay, G.; Shehzad, F.; Al-Harthi, M.A. Recent progress in layered double hydroxides (LDH)-containing hybrids as adsorbents for water remediation. *Appl. Clay Sci.* **2017**, *143*, 279–292. [CrossRef]

36. Das, T.K.; Ganguly, S.; Bhawal, P.; Remanan, S.; Mondal, S.; Das, N.C. Mussel inspired green synthesis of silver nanoparticles-decorated halloysite nanotube using dopamine: Characterization and evaluation of its catalytic activity. *Appl. Nanosci.* **2018**, *8*, 173–186. [CrossRef]
37. Chuaicham, C.; Xiong, Y.; Sekar, K.; Chen, W.; Zhang, L.; Ohtani, B.; Dabo, I.; Sasaki, K. A promising Zn-Ti layered double hydroxide/Fe-bearing montmorillonite composite as an efficient photocatalyst for Cr(VI) reduction: Insight into the role of Fe impurity in montmorillonite. *Appl. Surf. Sci.* **2021**, *546*, 148835. [CrossRef]
38. Dong, Y.; Liu, Z.; Chen, L. Removal of Zn(II) from aqueous solution by natural halloysite nanotubes. *J. Radioanal. Nucl. Chem.* **2012**, *292*, 435–443. [CrossRef]
39. Mogyorósi, K.; Farkas, A.; Dékány, I.; Ilisz, I.; Dombi, A. TiO_2-Based Photocatalytic Degradation of 2-Chlorophenol Adsorbed on Hydrophobic Clay. *Environ. Sci. Technol.* **2002**, *36*, 3618–3624. [CrossRef]
40. Kameshima, Y.; Tamura, Y.; Nakajima, A.; Okada, K. Preparation and properties of TiO_2/montmorillonite composites. *Appl. Clay Sci.* **2009**, *45*, 20–23. [CrossRef]
41. Papoulis, D.; Komarneni, S.; Nikolopoulou, A.; Tsolis-Katagas, P.; Panagiotaras, D.; Kacandes, H.G.; Zhang, P.; Yin, S.; Sato, T.; Katsuki, H. Palygorskite- and Halloysite-TiO_2 nanocomposites: Synthesis and photocatalytic activity. *Appl. Clay Sci.* **2010**, *50*, 118–124. [CrossRef]
42. Papoulis, D.; Komarneni, S.; Panagiotaras, D.; Stathatos, E.; Toli, D.; Christoforidis, K.C.; Fernández-García, M.; Li, H.; Yin, S.; Sato, T.; et al. Halloysite–TiO_2 nanocomposites: Synthesis, characterization and photocatalytic activity. *Appl. Catal. B Environ.* **2013**, *132–133*, 416–422. [CrossRef]
43. Rhouta, B.; Bouna, L.; Maury, F.; Senocq, F.; Lafont, M.C.; Jada, A.; Amjoud, M.; Daoudi, L. Surfactant-modifications of Na^+–beidellite for the preparation of TiO_2–Bd supported photocatalysts: II—Physico-chemical characterization and photocatalytic properties. *Appl. Clay Sci.* **2015**, *115*, 266–274. [CrossRef]
44. Khumchoo, N.; Khaorapapong, N.; Ontam, A.; Intachai, S.; Ogawa, M. Efficient Photodegradation of Organics in Acidic Solution by ZnO–Smectite Hybrids. *Eur. J. Inorg. Chem.* **2016**, *2016*, 3157–3162. [CrossRef]
45. Paiva, J.P.; Santos, B.A.M.C.; Kibwila, D.M.; Gonçalves, T.C.W.; Pinto, A.V.; Rodrigues, C.R.; Leitão, A.C.; Cabral, L.M.; Pádula, M.D. Titanium Dioxide–Montmorillonite Nanocomposite as Photoprotective Agent Against Ultraviolet B Radiation-Induced Mutagenesis in Saccharomyces cerevisiae: A Potential Candidate for Safer Sunscreens. *J. Pharm. Sci.* **2014**, *103*, 2539–2545. [CrossRef]
46. Tahir, M.; Amin, N.S. Photocatalytic reduction of carbon dioxide with water vapors over montmorillonite modified TiO_2 nanocomposites. *Appl. Catal. B Environ.* **2013**, *142–143*, 512–522. [CrossRef]
47. Jeong, E.; Lim, J.W.; Seo, K.-W.; Lee, Y.-S. Effects of physicochemical treatments of illite on the thermo-mechanical properties and thermal stability of illite/epoxy composites. *J. Ind. Eng. Chem.* **2011**, *17*, 77–82. [CrossRef]
48. Zhuang, G.; Zhang, Z.; Guo, J.; Liao, L.; Zhao, J. A new ball milling method to produce organo-montmorillonite from anionic and nonionic surfactants. *Appl. Clay Sci.* **2015**, *104*, 18–26. [CrossRef]
49. Li, Z.; Chen, M.; Ai, Z.; Wu, L.; Zhang, Q. Mechanochemical synthesis of CdS/MgAl LDH-precursor as improved visible-light driven photocatalyst for organic dye. *Appl. Clay Sci.* **2018**, *163*, 265–272. [CrossRef]
50. Xue, B.; Yang, K.; Wang, X.; Chi, Q.; Jiang, Y. The role of potassium chlorate on expansion of dickite layers and the preparation of a novel TiO_2 impregnated dickite photocatalyst using expanded dickite as carrier. *RSC Adv.* **2016**, *6*, 9803–9811. [CrossRef]
51. Zhu, T.T.; Zhou, C.H.; Kabwe, F.B.; Wu, Q.Q.; Li, C.S.; Zhang, J.R. Exfoliation of montmorillonite and related properties of clay/polymer nanocomposites. *Appl. Clay Sci.* **2019**, *169*, 48–66. [CrossRef]
52. Ong, W.-J.; Tan, L.-L.; Ng, Y.H.; Yong, S.-T.; Chai, S.-P. Graphitic Carbon Nitride (g-C_3N_4)-Based Photocatalysts for Artificial Photosynthesis and Environmental Remediation: Are We a Step Closer To Achieving Sustainability? *Chem. Rev.* **2016**, *116*, 7159–7329. [CrossRef]
53. Mishra, A.; Mehta, A.; Basu, S.; Shetti, N.P.; Reddy, K.R.; Aminabhavi, T.M. Graphitic carbon nitride (g–C_3N_4)–based metal-free photocatalysts for water splitting: A review. *Carbon* **2019**, *149*, 693–721. [CrossRef]
54. Wen, J.; Xie, J.; Chen, X.; Li, X. A review on g-C_3N_4-based photocatalysts. *Appl. Surf. Sci.* **2017**, *391*, 72–123. [CrossRef]
55. Fu, J.; Yu, J.; Jiang, C.; Cheng, B. g-C_3N_4-Based Heterostructured Photocatalysts. *Adv. Energy Mater.* **2018**, *8*, 1701503. [CrossRef]
56. Jiang, H.; Li, Y.; Wang, D.; Hong, X.; Liang, B. Recent Advances in Heteroatom Doped Graphitic Carbon Nitride (g-C_3N_4) and g-C_3N_4/Metal Oxide Composite Photocatalysts. *Curr. Org. Chem.* **2020**, *24*, 673–693. [CrossRef]
57. Wu, J.; Li, N.; Zhang, X.-H.; Fang, H.-B.; Zheng, Y.-Z.; Tao, X. Heteroatoms binary-doped hierarchical porous g-C_3N_4 nanobelts for remarkably enhanced visible-light-driven hydrogen evolution. *Appl. Catal. B Environ.* **2018**, *226*, 61–70. [CrossRef]
58. Humayun, M.; Ullah, H.; Shu, L.; Ao, X.; Tahir, A.A.; Wang, C.; Luo, W. Plasmon Assisted Highly Efficient Visible Light Catalytic CO_2 Reduction Over the Noble Metal Decorated Sr-Incorporated g-C_3N_4. *Nano-Micro Lett.* **2021**, *13*, 209. [CrossRef]
59. Humayun, M.; Fu, Q.; Zheng, Z.; Li, H.; Luo, W. Improved visible-light catalytic activities of novel Au/P-doped g-C_3N_4 photocatalyst for solar fuel production and mechanism. *Appl. Catal. A Gen.* **2018**, *568*, 139–147. [CrossRef]
60. He, C.; Zhang, J.H.; Zhang, W.X.; Li, T.T. Type-II InSe/g-C_3N_4 Heterostructure as a High-Efficiency Oxygen Evolution Reaction Catalyst for Photoelectrochemical Water Splitting. *J. Phys. Chem. Lett.* **2019**, *10*, 3122–3128. [CrossRef]
61. Zhao, X.; You, Y.; Huang, S.; Wu, Y.; Ma, Y.; Zhang, G.; Zhang, Z. Z-scheme photocatalytic production of hydrogen peroxide over $Bi_4O_5Br_2$/g-C_3N_4 heterostructure under visible light. *Appl. Catal. B Environ.* **2020**, *278*, 119251. [CrossRef]

62. Yang, Y.; Yang, F.; Li, Z.; Zhang, N.; Hao, S. Z-scheme g-C_3N_4/C/S-g-C_3N_4 heterostructural nanotube with enhanced porous structure and visible light driven photocatalysis. *Microporous Mesoporous Mater.* **2021**, *314*, 110891. [CrossRef]
63. Ma, W.; Wang, N.; Guo, Y.; Yang, L.; Lv, M.; Tang, X.; Li, S. Enhanced photoreduction CO_2 activity on g-C_3N_4: By synergistic effect of nitrogen defective-enriched and porous structure, and mechanism insights. *Chem. Eng. J.* **2020**, *388*, 124288. [CrossRef]
64. Chuaicham, C.; Pawar, R.; Sasaki, K. Dye-sensitized Photocatalyst of Sepiolite for Organic Dye Degradation. *Catalysts* **2019**, *9*, 235. [CrossRef]
65. Li, C.; Zhu, N.; Yang, S.; He, X.; Zheng, S.; Sun, Z.; Dionysiou, D.D. A review of clay based photocatalysts: Role of phyllosilicate mineral in interfacial assembly, microstructure control and performance regulation. *Chemosphere* **2021**, *273*, 129723. [CrossRef]
66. Qin, W.-L.; Lv, H.; Xia, T.; Ye, Y.; Chen, X.-G.; Lyu, S.-S. TiO_2 Intercalated Talc Nanocomposite: Preparation, Characterization, and Its Photocatalytic Performance. *J. Nanosci. Nanotechnol.* **2017**, *17*, 6558–6565. [CrossRef]
67. Sun, Z.; Yao, G.; Zhang, X.; Zheng, S.; Frost, R.L. Enhanced visible-light photocatalytic activity of kaolinite/g-C_3N_4 composite synthesized via mechanochemical treatment. *Appl. Clay Sci.* **2016**, *129*, 7–14. [CrossRef]
68. Sun, Z.; Yuan, F.; Li, X.; Li, C.; Xu, J.; Wang, B. Fabrication of Novel Cyanuric Acid Modified g-C_3N_4/Kaolinite Composite with Enhanced Visible Light-Driven Photocatalytic Activity. *Minerals* **2018**, *8*, 437.
69. Li, C.; Sun, Z.; Zhang, W.; Yu, C.; Zheng, S. Highly efficient g-C_3N_4/TiO_2/kaolinite composite with novel three-dimensional structure and enhanced visible light responding ability towards ciprofloxacin and *S. aureus*. *Appl. Catal. B Environ.* **2018**, *220*, 272–282. [CrossRef]
70. Cao, Z.; Jia, Y.; Wang, Q.; Cheng, H. High-efficiency photo-Fenton Fe/g-C_3N_4/kaolinite catalyst for tetracycline hydrochloride degradation. *Appl. Clay Sci.* **2021**, *212*, 106213. [CrossRef]
71. Wang, X.; Zhao, Z.; Shu, Z.; Chen, Y.; Zhou, J.; Li, T.; Wang, W.; Tan, Y.; Sun, N. One-pot synthesis of metakaolin/g-C_3N_4 composite for improved visible-light photocatalytic H2 evolution. *Appl. Clay Sci.* **2018**, *166*, 80–87. [CrossRef]
72. Zhu, Z.; Yu, Y.; Dong, H.; Liu, Z.; Li, C.; Huo, P.; Yan, Y. Intercalation Effect of Attapulgite in g-C_3N_4 Modified with Fe_3O_4 Quantum Dots To Enhance Photocatalytic Activity for Removing 2-Mercaptobenzothiazole under Visible Light. *ACS Sustain. Chem. Eng.* **2017**, *5*, 10614–10623. [CrossRef]
73. Xie, H.; Zhang, J.; Wang, D.; Liu, J.; Wang, L.; Xiao, H. Construction of three-dimensional g-C_3N_4/attapulgite hybrids for Cd(II) adsorption and the reutilization of waste adsorbent. *Appl. Surf. Sci.* **2020**, *504*, 144456. [CrossRef]
74. Xu, Y.; Zhang, L.; Chen, J.; Fu, Y.; Li, Q.; Yin, J.; Cheng, Z.; Kan, W.; Zhao, P.; Zhong, H.; et al. Synthesis of nano-Ag-assisted attapulgite/g-C_3N_4 composites with superior visible light photocatalytic performance. *Mater. Chem. Phys.* **2019**, *221*, 447–456. [CrossRef]
75. Li, J.; Zhou, M.; Ye, Z.; Wang, H.; Ma, C.; Huo, P.; Yan, Y. Enhanced photocatalytic activity of g-C_3N_4–ZnO/HNT composite heterostructure photocatalysts for degradation of tetracycline under visible light irradiation. *RSC Adv.* **2015**, *5*, 91177–91189. [CrossRef]
76. Hojamberdiev, M.; Khan, M.M.; Kadirova, Z.; Kawashima, K.; Yubuta, K.; Teshima, K.; Riedel, R.; Hasegawa, M. Synergistic effect of g-C_3N_4, $Ni(OH)_2$ and halloysite in nanocomposite photocatalyst on efficient photocatalytic hydrogen generation. *Renew. Energy* **2019**, *138*, 434–444. [CrossRef]
77. Li, C.; Sun, Z.; Huang, W.; Zheng, S. Facile synthesis of g-C_3N_4/montmorillonite composite with enhanced visible light photodegradation of rhodamine B and tetracycline. *J. Taiwan Inst. Chem. Eng.* **2016**, *66*, 363–371. [CrossRef]
78. Xu, J.; Qi, Y.; Wang, W.; Wang, L. Montmorillonite-hybridized g-C_3N_4 composite modified by NiCoP cocatalyst for efficient visible-light-driven photocatalytic hydrogen evolution by dye-sensitization. *Int. J. Hydrogen Energy* **2019**, *44*, 4114–4122. [CrossRef]
79. Wan, X.; Khan, M.A.; Wang, F.; Xia, M.; Lei, W.; Zhu, S.; Fu, C.; Ding, Y. Facile synthesis of protonated g-C_3N_4 and acid-activated montmorillonite composite with efficient adsorption capacity for $PO4^{3-}$ and Pb(II). *Chem. Eng. Res. Des.* **2019**, *152*, 95–105. [CrossRef]
80. Sun, Z.; Zhang, X.; Zhu, R.; Dong, X.; Xu, J.; Wang, B. Facile Synthesis of Visible Light-Induced g-C_3N_4/Rectorite Composite for Efficient Photodegradation of Ciprofloxacin. *Materials* **2018**, *11*, 2452.
81. Zhu, L.; Zhou, P.-J.; Chen, C. g-C_3N_4/rectorite as a highly efficient catalyst for peroxymonosulfate activation to remove organic contaminants in water. *J. Environ. Chem. Eng.* **2022**, *10*, 107168. [CrossRef]
82. Chuaicham, C.; Pawar, R.R.; Karthikeyan, S.; Ohtani, B.; Sasaki, K. Fabrication and characterization of ternary sepiolite/g-C_3N_4/Pd composites for improvement of photocatalytic degradation of ciprofloxacin under visible light irradiation. *J. Colloid Interface Sci.* **2020**, *577*, 397–405. [CrossRef]
83. Fan, E.; Hu, F.; Miao, W.; Xu, H.; Shao, G.; Liu, W.; Li, M.; Wang, H.; Lu, H.; Zhang, R. Preparation of g-C_3N_4/vermiculite composite with improved visible light photocatalytic activity. *Appl. Clay Sci.* **2020**, *197*, 105789. [CrossRef]
84. Chen, Y.; Wen, L.; Chen, J.; Luo, H.A.; Liu, J. In situ growth of g-C_3N_4 on clay minerals of kaolinite, sepiolite, and talc for enhanced solar photocatalytic energy conversion. *Appl. Clay Sci.* **2022**, *216*, 106337. [CrossRef]
85. Bakbolat, B.; Daulbayev, C.; Sultanov, F.; Beissenov, R.; Umirzakov, A.; Mereke, A.; Bekbaev, A.; Chuprakov, I. Recent Developments of TiO_2-Based Photocatalysis in the Hydrogen Evolution and Photodegradation: A Review. *Nanomaterials* **2020**, *10*, 1790. [CrossRef]
86. Guo, Q.; Zhou, C.; Ma, Z.; Yang, X. Fundamentals of TiO_2 Photocatalysis: Concepts, Mechanisms, and Challenges. *Adv. Mater.* **2019**, *31*, e1901997. [CrossRef]

87. Wang, Y.; Gong, Y.; Lin, N.; Yu, L.; Du, B.; Zhang, X. Enhanced removal of Cr (VI) from aqueous solution by stabilized nanoscale zero valent iron and copper bimetal intercalated montmorillonite. *J. Colloid Interface Sci.* **2022**, *606*, 941–952. [CrossRef]
88. Chen, D.; Zhu, Q.; Zhou, F.; Deng, X.; Li, F. Synthesis and photocatalytic performances of the TiO_2 pillared montmorillonite. *J. Hazard. Mater.* **2012**, *235*, 186–193.
89. Zhang, L.; Chuaicham, C.; Balakumar, V.; Sekar, K.; Ohtani, B.; Sasaki, K. Determination of the roles of FeIII in the interface between titanium dioxide and montmorillonite in FeIII-doped montmorillonite/titanium dioxide composites as photocatalysts. *Appl. Clay Sci.* **2022**, *227*, 106577. [CrossRef]
90. Belessi, V.; Lambropoulou, D.; Konstantinou, I.; Katsoulidis, A.; Pomonis, P.; Petridis, D.; Albanis, T. Structure and photocatalytic performance of TiO_2/clay nanocomposites for the degradation of dimethachlor. *Appl. Catal. B Environ.* **2007**, *73*, 292–299. [CrossRef]
91. Mahy, J.G.; Tsaffo Mbognou, M.H.; Léonard, C.; Fagel, N.; Woumfo, E.D.; Lambert, S.D. Natural Clay Modified with ZnO/TiO_2 to Enhance Pollutant Removal from Water. *Catalysts* **2022**, *12*, 148. [CrossRef]
92. Shirzad-Siboni, M.; Farrokhi, M.; Darvishi Cheshmeh Soltani, R.; Khataee, A.; Tajassosi, S. Photocatalytic reduction of hexavalent chromium over ZnO nanorods immobilized on kaolin. *Ind. Eng. Chem. Res.* **2014**, *53*, 1079–1087. [CrossRef]
93. Li, C.; Zhu, N.; Dong, X.; Zhang, X.; Chen, T.; Zheng, S.; Sun, Z. Tuning and controlling photocatalytic performance of TiO_2/kaolinite composite towards ciprofloxacin: Role of 0D/2D structural assembly. *Adv. Powder Technol.* **2020**, *31*, 1241–1252. [CrossRef]
94. Li, X.; Peng, K.; Chen, H.; Wang, Z. TiO_2 nanoparticles assembled on kaolinites with different morphologies for efficient photocatalytic performance. *Sci. Rep.* **2018**, *8*, 11663.
95. Kutláková, K.M.; Tokarský, J.; Kovář, P.; Vojtěšková, S.; Kovářová, A.; Smetana, B.; Kukutschová, J.; Čapková, P.; Matějka, V. Preparation and characterization of photoactive composite kaolinite/TiO_2. *J. Hazard. Mater.* **2011**, *188*, 212–220.
96. Zhang, Y.; Gan, H.; Zhang, G. A novel mixed-phase TiO_2/kaolinite composites and their photocatalytic activity for degradation of organic contaminants. *Chem. Eng. J.* **2011**, *172*, 936–943.
97. Wu, A.; Wang, D.; Wei, C.; Zhang, X.; Liu, Z.; Feng, P.; Ou, X.; Qiang, Y.; Garcia, H.; Niu, J. A comparative photocatalytic study of TiO_2 loaded on three natural clays with different morphologies. *Appl. Clay Sci.* **2019**, *183*, 105352. [CrossRef]
98. Djellabi, R.; Fouzi Ghorab, M.; Bianchi, C.L.; Cerrato, G.; Morandi, S. Removal of crystal violet and hexavalent chromium using TiO_2-bentonite under sunlight: Effect of TiO_2 content. *J. Chem. Eng. Process. Technol.* **2016**, *7*, 1000276.
99. Yang, C.; Zhu, Y.; Wang, J.; Li, Z.; Su, X.; Niu, C. Hydrothermal synthesis of TiO_2–WO_3–bentonite composites: Conventional versus ultrasonic pretreatments and their adsorption of methylene blue. *Appl. Clay Sci.* **2015**, *105*, 243–251. [CrossRef]
100. Dallabona, I.D.; Mathias, Á.L.; Jorge, R.M.M. A new green floating photocatalyst with Brazilian bentonite into TiO_2/alginate beads for dye removal. *Colloids Surf. A Physicochem. Eng. Asp.* **2021**, *627*, 127159. [CrossRef]
101. Sun, Q.; Hu, X.; Zheng, S.; Sun, Z.; Liu, S.; Li, H. Influence of calcination temperature on the structural, adsorption and photocatalytic properties of TiO_2 nanoparticles supported on natural zeolite. *Powder Technol.* **2015**, *274*, 88–97.
102. Sun, Z.; Zheng, L.; Zheng, S.; Frost, R.L. Preparation and characterization of TiO_2/acid leached serpentinite tailings composites and their photocatalytic reduction of Chromium (VI). *J. Colloid Interface Sci.* **2013**, *404*, 102–109. [CrossRef]
103. Yang, Y.; Yan, L.; Li, J.; Li, J.; Yan, T.; Sun, M.; Pei, Z. Synergistic adsorption and photocatalytic reduction of Cr (VI) using Zn-Al-layered double hydroxide and TiO_2 composites. *Appl. Surf. Sci.* **2019**, *492*, 487–496.
104. Li, F.; Dai, Y.; Gong, M.; Yu, T.; Chen, X. Synthesis, characterization of magnetic-sepiolite supported with TiO_2, and the photocatalytic performance over Cr (VI) and 2,4-dichlorophenol co-existed wastewater. *J. Alloys Compd.* **2015**, *638*, 435–442. [CrossRef]
105. Dvininov, E.; Popovici, E.; Pode, R.; Cocheci, L.; Barvinschi, P.; Nica, V. Synthesis and characterization of TiO_2-pillared Romanian clay and their application for azoic dyes photodegradation. *J. Hazard. Mater.* **2009**, *167*, 1050–1056. [CrossRef]
106. Sun, Z.; Hu, Z.; Yan, Y.; Zheng, S. Effect of preparation conditions on the characteristics and photocatalytic activity of TiO_2/purified diatomite composite photocatalysts. *Appl. Surf. Sci.* **2014**, *314*, 251–259.
107. Ramadan, H.; Ali, R.A.; Mobarak, M.; Badawi, M.; Selim, A.Q.; Mohamed, E.A.; Bonilla-Petriciolet, A.; Seliem, M.K. One-step fabrication of a new outstanding rutile TiO_2 nanoparticles/anthracite adsorbent: Modeling and physicochemical interpretations for malachite green removal. *Chem. Eng. J.* **2021**, *426*, 131890.
108. Savun-Hekimoğlu, B.; Eren, Z.; Ince, N.H. Photocatalytic Destruction of Caffeine on Sepiolite-Supported TiO_2 Nanocomposite. *Sustainability* **2020**, *12*, 10314. [CrossRef]
109. Zhang, Y.; Miao, B.; Chen, Q.; Bai, Z.; Cao, Y.; Davaa, B. Synthesis, Structure, and Photocatalytic Activity of TiO_2-Montmorillonite Composites. *Catalysts* **2022**, *12*, 486. [CrossRef]
110. Sreekala, S.V.; Vayalveettil, A.; Kochu, J.K.; Ramakrishnan, R.T.; Pillai, H.P.S. Bentonite-titanium dioxide functional nanocomposites suitable for wastewater treatment: An integrated photocatalyst-adsorbent system. *New J. Chem.* **2022**, *46*, 4772–4783. [CrossRef]
111. Keller, W.D.; Matlack, K. The pH of clay suspensions in the field and laboratory, and methods of measurement of their pH. *Appl. Clay Sci.* **1990**, *5*, 123–133. [CrossRef]
112. Tun, P.P.; Wang, J.; Khaing, T.T.; Wu, X.; Zhang, G. Fabrication of functionalized plasmonic Ag loaded Bi_2O_3/montmorillonite nanocomposites for efficient photocatalytic removal of antibiotics and organic dyes. *J. Alloys Compd.* **2020**, *818*, 152836. [CrossRef]

113. Xu, C.; Wu, H.; Gu, F.L. Efficient adsorption and photocatalytic degradation of Rhodamine B under visible light irradiation over BiOBr/montmorillonite composites. *J. Hazard. Mater.* **2014**, *275*, 185–192. [CrossRef]
114. Naing, H.H.; Li, Y.; Ghasemi, J.B.; Wang, J.; Zhang, G. Enhanced visible-light-driven photocatalysis of in-situ reduced of bismuth on BiOCl nanosheets and montmorillonite loading: Synergistic effect and mechanism insight. *Chemosphere* **2022**, *304*, 135354. [CrossRef]
115. Xu, C.; Gu, F.L.; Wu, H. BiOCl-montmorillonite as a photocatalyst for highly efficient removal of Rhodamine B and Orange G: Importance of the acidity and dissolved oxygen. *Appl. Clay Sci.* **2017**, *147*, 28–35. [CrossRef]
116. Xu, T.; Zhu, R.; Zhu, J.; Liang, X.; Liu, Y.; Xu, Y.; He, H. $BiVO_4$/Fe/Mt composite for visible-light-driven degradation of acid red 18. *Appl. Clay Sci.* **2016**, *129*, 27–34. [CrossRef]
117. Landge, V.K.; Sonawane, S.H.; Sivakumar, M.; Sonawane, S.S.; Babu, G.U.B.; Boczkaj, G. S-scheme heterojunction Bi_2O_3-ZnO/Bentonite clay composite with enhanced photocatalytic performance. *Sustain. Energy Technol. Assess.* **2021**, *45*, 101194. [CrossRef]
118. Dlamini, M.C.; Dlamini, M.L.; Mente, P.; Tlhaole, B.; Erasmus, R.; Maubane-Nkadimeng, M.S.; Moma, J.A. Photocatalytic abatement of phenol on amorphous TiO_2-BiOBr-bentonite heterostructures under visible light irradiation. *J. Ind. Eng. Chem.* **2022**, *111*, 419–436. [CrossRef]
119. Vaizoğullar, A.İ. Synthesis, characterization, and photocatalytic activities of novel bentonite-supported BiOCl–ZnO heterojunction (BiOCl–ZnO–Bentonite) under UV light. *Asia Pac. J. Chem. Eng.* **2018**, *13*, e2154. [CrossRef]
120. Hu, X.; Li, C.; Song, J.; Zheng, S.; Sun, Z. Hierarchical assembly of visible-light-driven Bi_2MoO_6/TiO_2/sepiolite composite for effective formaldehyde removal. *Appl. Clay Sci.* **2022**, *227*, 106590. [CrossRef]
121. Naing, H.H.; Wang, K.; Li, Y.; Mishra, A.K.; Zhang, G. Sepiolite supported $BiVO_4$ nanocomposites for efficient photocatalytic degradation of organic pollutants: Insight into the interface effect towards separation of photogenerated charges. *Sci. Total Environ.* **2020**, *722*, 137825. [CrossRef]
122. Wang, J.; Fan, J.; Li, J.; Wu, X.; Zhang, G. Ultrasound assisted synthesis of Bi_2NbO_5F/rectorite composite and its photocatalytic mechanism insights. *Ultrason. Sonochemistry* **2018**, *48*, 404–411. [CrossRef]
123. Chuaicham, C.; Sekar, K.; Balakumar, V.; Uchida, J.; Katsurao, T.; Sakabe, H.; Ohtani, B.; Sasaki, K. Efficient photocatalytic degradation of emerging ciprofloxacin under visible light irradiation using BiOBr/carbon quantum dot/saponite composite. *Environ. Res.* **2022**, *212*, 113635. [CrossRef]
124. Luo, Y.; Wang, K.; Hu, T.; Liu, X. Controlled synthesis of palygorskite/Bi_5O_7I hybrid microspheres with high efficient photodegradation of antibiotics. *Colloids Surf. A Physicochem. Eng. Asp.* **2021**, *616*, 126225. [CrossRef]
125. Liu, J.; Jatav, S.; Wessel, P.; Hill, E.H. Templating Unidirectional Bismuth Oxyiodide Crystal Growth with Layered Silicates for Enhanced Photocatalysis. *J. Phys. Chem. C* **2022**, *126*, 4975–4983. [CrossRef]
126. Tun, P.; Wang, K.; Naing, H.; Wang, J.; Zhang, G. Facile preparation of visible-light-responsive kaolin-supported Ag@AgBr composites and their enhanced photocatalytic properties. *Appl. Clay Sci.* **2019**, *175*, 76–85. [CrossRef]
127. Li, Z.; Zhang, Q.; Liu, X.; Wu, L.; Hu, H.; Zhao, Y. One-step mechanochemical synthesis of plasmonic Ag/Zn–Al LDH with excellent photocatalytic activity. *J. Mater. Sci.* **2018**, *53*, 12795–12806. [CrossRef]
128. Pham, M.-T.; Hussain, A.; Bui, D.-P.; Nguyen, T.-M.T.; You, S.-J.; Wang, Y.-F. Surface plasmon resonance enhanced photocatalysis of Ag nanoparticles-decorated Bi_2S_3 nanorods for NO degradation. *Environ. Technol. Innov.* **2021**, *23*, 101755. [CrossRef]
129. Mishra, A.; Mehta, A.; Kainth, S.; Basu, S. Effect of different plasmonic metals on photocatalytic degradation of volatile organic compounds (VOCs) by bentonite/M-TiO_2 nanocomposites under UV/visible light. *Appl. Clay Sci.* **2018**, *153*, 144–153. [CrossRef]
130. Praneeth, N.V.S.; Paria, S. Clay-supported anisotropic Au-modified N,S-doped TiO_2 nanoparticles for enhanced photocatalytic dye degradation and esterification reactions. *New J. Chem.* **2020**, *44*, 2619–2629. [CrossRef]
131. Kaur, H.; Singh, S.; Pal, B. Effect of plasmonic metal (Cu, Ag, and Au) loading over the physicochemical and photocatalytic properties of Mg-Al LDH towards degradation of tetracycline under LED light. *Appl. Surf. Sci.* **2023**, *609*, 155455. [CrossRef]
132. Tonda, S.; Jo, W.-K. Plasmonic Ag nanoparticles decorated NiAl-layered double hydroxide/graphitic carbon nitride nanocomposites for efficient visible-light-driven photocatalytic removal of aqueous organic pollutants. *Catal. Today* **2018**, *315*, 213–222. [CrossRef]
133. Shabib, F.; Fazaeli, R.; Aliyan, H.; Richeson, D. Hierarchical mesoporous plasmonic Pd-Fe_3O_4/NiFe-LDH composites: Characterization, and kinetic study of a photodegradation catalyst for aqueous metoclopramide. *Environ. Technol. Innov.* **2022**, *27*, 102515. [CrossRef]
134. Pawar, R.R.; Chuaicham, C.; Sekar, K.; Rajendran, S.; Sasaki, K. Synthesis, characterization, and application of MOF@clay composite as a visible light-driven photocatalyst for Rhodamine B degradation. *Chemosphere* **2022**, *291*, 132922. [CrossRef]
135. Bhuvaneswari, K.; Palanisamy, G.; Pazhanivel, T.; Maiyalagan, T.; Shanmugam, P.; Grace, A.N. In-situ development of metal organic frameworks assisted ZnMgAl layered triple hydroxide 2D/2D hybrid as an efficient photocatalyst for organic dye degradation. *Chemosphere* **2021**, *270*, 128616. [CrossRef]
136. Liu, S.; Jiang, X.; Waterhouse, G.I.N.; Zhang, Z.-M.; Yu, L.-m. Construction of Z-scheme Titanium-MOF/plasmonic silver nanoparticle/NiFe layered double hydroxide photocatalysts with enhanced dye and antibiotic degradation activity under visible light. *Sep. Purif. Technol.* **2021**, *278*, 119525. [CrossRef]

137. Wang, T.; Yang, Y.; Deng, Q.; Zhang, X.; Xiong, L.; Tang, Z.; Li, P.; Yin, N.; Sun, A.; Chen, D.; et al. In-situ construction of 3D marigold-like CoAl-LDH/Ti_3C_2 heterosystem collaborating with 2D/2D interface for efficient photodegradation of multiple antibiotics. *Appl. Surf. Sci.* **2021**, *569*, 151084. [CrossRef]
138. Ma, Y.; Xu, D.; Chen, W.; Tang, Y.; Wang, X.; Li, L.; Wang, J. Oxygen-vacancy-embedded 2D/2D NiFe-LDH/MXene Schottky heterojunction for boosted photodegradation of norfloxacin. *Appl. Surf. Sci.* **2022**, *572*, 151432. [CrossRef]
139. Grzegórska, A.; Wysocka, I.; Głuchowski, P.; Ryl, J.; Karczewski, J.; Zielińska-Jurek, A. Novel composite of Zn/Ti-layered double hydroxide coupled with MXene for the efficient photocatalytic degradation of pharmaceuticals. *Chemosphere* **2022**, *308*, 136191. [CrossRef]
140. Yang, J.; Jing, R.; Wang, P.; Liang, D.; Huang, H.; Xia, C.; Zhang, Q.; Liu, A.; Meng, Z.; Liu, Y. Black phosphorus nanosheets and ZnAl-LDH nanocomposite as environmental-friendly photocatalysts for the degradation of Methylene blue under visible light irradiation. *Appl. Clay Sci.* **2021**, *200*, 105902. [CrossRef]
141. Amani-Ghadim, A.R.; Khodam, F.; Seyed Dorraji, M.S. ZnS quantum dot intercalated layered double hydroxide semiconductors for solar water splitting and organic pollutant degradation. *J. Mater. Chem. A* **2019**, *7*, 11408–11422. [CrossRef]
142. Khodam, F.; Amani-Ghadim, A.R.; Ashan, N.N.; Sareshkeh, A.T.; Bayat, F.; Gholinejad, M.; Dorraji, M.S.S. CdTe quantum dots incorporated in CoNiAl layered double hydroxide interlayer spaces as a highly efficient visible light driven photocatalyst for degradation of an azo dye and Bisphenol A. *J. Alloys Compd.* **2022**, *898*, 162768. [CrossRef]
143. Ganguly, S.; Das, P.; Das, T.K.; Ghosh, S.; Das, S.; Bose, M.; Mondal, M.; Das, A.K.; Das, N.C. Acoustic cavitation assisted destratified clay tactoid reinforced in situ elastomer-mimetic semi-IPN hydrogel for catalytic and bactericidal application. *Ultrason. Sonochemistry* **2020**, *60*, 104797. [CrossRef]

Disclaimer/Publisher's Note: The statements, opinions and data contained in all publications are solely those of the individual author(s) and contributor(s) and not of MDPI and/or the editor(s). MDPI and/or the editor(s) disclaim responsibility for any injury to people or property resulting from any ideas, methods, instructions or products referred to in the content.